The DNA Damage response and cell competition are p53- and Xrp1-dependent processes that suppress hyperplastic aneuploidy

Chaitali Khan[1] and Nicholas E. Baker[2]

Department of Genetics
Albert Einstein College of Medicine
1300 Morris Park Avenue
Bronx
NY 10461
USA

1. Present address: Cell and Developmental Biology Center, National Heart Lung and Blood Institute, National Institutes of Health, Bethesda, MD 20892, USA

2. Author for correspondence: Nicholas.baker@einsteinmed.edu

ABSTRACT

It is important to understand how p53 suppresses tumorigenesis. P53 activity contributes to many instances of cell competition in mammals. This has not been seen for *Drosophila* p53, where the transcription factor Xrp1 is an effector of cell competition. Xrp1 is induced in a p53-dependent manner by DNA damage, and we report that Xrp1 mediates multiple functions of p53 in the DNA damage response, contributing to p53-dependent gene transcription and DNA damage-induced apoptosis. Differences in either Xrp1 or p53 activity, occurring between wild type and mutant cells experiencing mild genotoxic stress, both resulted in cell competition. Unexpectedly, cell competition due to differential p53 activity did not require Xrp1 but instead was restrained by Xrp1. We show that Xrp1 has a p53-independent role in removing genomically-altered cells. Both Xrp1 and p53 limit the accumulation of abnormal cells that results from genotoxicity, and we propose that genomic alterations enhance cellular growth of p53 mutant cells and promote cell competition, potentially contributing to the tumorigenesis in p53 mutants.

INTRODUCTION

Mutations in the tumor suppressor gene p53 occur frequently in many cancer types (Muller and Vousden 2014). This comes as no surprise since p53 plays an essential role in ensuring genomic integrity by serving as the key effector of DNA damage response (DDR) (Levine, Hu, and Feng 2006; Kastenhuber and Lowe 2017). However, the emphasis on p53's role in DDR as its tumor suppression mechanism has recently been questioned. Point mutations that block p53 function in the acute DDR have little effect in blocking tumor growth, and conditional knock-out studies point to a critical window for tumor suppressor function that is subsequent to the resolution of DNA damage (Christophorou et al. 2005; Christophorou et al. 2006; Li et al. 2012; Kaiser and Attardi 2018). Besides responding to DNA damage, p53 has other functions ranging from metabolic regulation, cell-cell recognition and cell competition (Baker 2020; Lacroix et al. 2020; Pilley, Rodriguez, and Vousden 2021). These other functions might also be important for tumor suppression by p53. Here we focus on the role of p53 in cell competition. Cell competition is a phenomenon whereby interaction between cells leads to the elimination of cells with lower fitness, and in mammals higher p53 activity is often associated with lower fitness (Merino et al. 2015; Nagata and Igaki 2018; Baker 2020; Morata 2021; Pilley, Rodriguez, and Vousden 2021). Cell competition was first described in the case of *Drosophila* cells heterozygous for mutations in ribosomal protein genes ($Rp^{+/-}$ cells) (Morata and Ripoll 1975). Cell competition is not limited to $Rp^{+/-}$ mutants but occurs in response to a variety of genetic differences, in mammals as well as in *Drosophila* (Maruyama and Fujita 2017; Baker 2017).

One function of cell competition is to suppress tumorigenesis by eliminating abnormal cells prior to transformation (Vishwakarma and Piddini 2020; Gogna and Moreno 2020). Indeed, cell competition removes *Drosophila* cells mutated for certain genes defining apical-basal polarity of epithelial cells, which otherwise form neoplastic tumors (Brumby and Richardson 2003; Igaki, Pagliarini, and Xu 2006; Kanda and Igaki 2020). In addition, our recent work demonstrated that ribosomal protein (Rp) genes participate in the recognition and removal of certain aneuploid cells through cell competition. Almost all tumors are aneuploid, and genotypes that promote aneuploidy are cancer prone in humans and in mouse models, therefore it is expected that mechanisms that reduce aneuploidy are tumor suppressive (Hanks et al. 2004; Matsuura et al. 2006; Foijer, Draviam, and Sorger 2008; García-Castillo et al. 2008; Baker et al. 2009; Snape et al. 2011;

83 Mukherjee et al. 2014). Because the *Rp* genes are distributed around the genome, in
84 *Drosophila* as in humans, aneuploidy and other large-scale genetic alterations generally
85 change *Rp* gene dose, and such changes could serve as a sensor for genomic alterations
86 (Uechi, Tanaka, and Kenmochi 2001; Marygold et al. 2007; McNamee and Brodsky 2009).
87 Accordingly, clones of cells with segmental chromosome deletions are only tolerated
88 when they do not affect *Rp* gene dose, but eliminated by cell competition when they
89 reduce dose of *Rp* genes (Ji et al. 2021).
90 Aneuploidy is also known to cause a stress response due to the altered expression
91 of many proteins, not just Rp, leading to cell-autonomous deficits in growth and survival
92 (Torres et al. 2007; Dekanty et al. 2012; Brennan et al. 2019; Joy et al. 2021). In *Drosophila*,
93 blocking apoptosis of the aneuploid cells that result from chromosome instability, and
94 which experience cell-autonomous stress, leads to invasive tumors (Dekanty et al. 2012;
95 Joy et al. 2021).
96 Differences in p53 activity between cells are a key feature of many instances of
97 cell competition in mammals, and by themselves are sufficient to lead to competition
98 between mammalian cells (Baker, Kiparaki, and Khan 2019; Pilley, Rodriguez, and
99 Vousden 2021). For example, in mouse hematopoietic stem cell chimeras, p53 activation
100 by low dose ionizing radiation leads to elimination of cells with higher relative levels of
101 p53 (Bondar and Medzhitov 2010; Marusyk et al. 2010). Similarly, in mouse embryo
102 chimeras, aneuploid cells are eliminated by the presence of euploid cells in a p53-
103 dependent manner (Singla et al. 2020). In cultured mammalian cells, direct
104 pharmacological activation of p53, in the absence of other stressors, is sufficient to
105 promote competitive elimination (Wagstaff et al. 2016).
106 Heterozygous mutation of human Rp genes activates p53 through inhibition of
107 MDM2 (Donati et al. 2011; Bursac et al. 2014). In *Drosophila*, there is no evidence that p53
108 is activated by Rp mutations, p53 is not required for the cell competition of $Rp^{+/-}$ cells, and
109 the MDM2 proteins, whose inhibition in mammalian p53 mutant cells is the basis for p53
110 activation, are absent from *Drosophila* (Chakraborty et al. 2015; Kale et al. 2015; Lee et al.
111 2018). There is, however, a role for p53 in protective metabolic changes that permit
112 *Drosophila* cells expressing elevated *myc* to eliminate nearby wild type cells. This is an
113 example of super-competition where it is the wild-type cells that are eliminated (de La
114 Cova et al. 2014).

115 Instead of p53, the transcription factor that is important in the competition of *Rp*$^{+/-}$
116 cells is the bZip domain protein Xrp1. Xrp1 protein is barely expressed in wild type
117 imaginal discs, but induced by *Rp* mutations (Lee et al. 2016; Baillon et al. 2018; Lee et al.
118 2018). Xrp1 expression is induced in *Rp*$^{+/-}$ cells not by p53 but through an activity of the
119 RpS12 protein; this activity seems to be enhanced in *Rp*$^{+/-}$ cells (Kale et al. 2018; Lee et al.
120 2018; Ji et al. 2019). Aneuploid cells that arise as a consequence of irradiation, or telomere
121 loss, are eliminated from *Drosophila* tissues in a p53-independent manner (Wichmann,
122 Jaklevic, and Su 2006; McNamee and Brodsky 2009; Titen and Golic 2008). The majority
123 of such aneuploid cell elimination depends on RpS12, suggesting that it represents a cell
124 competition process similar to that affecting *Rp*$^{+/-}$ cells (Ji et al. 2021). Xrp1 binds to DNA
125 as a heterodimer with another bZip protein, Irbp18, as originally discovered though
126 binding of Xrp1 and Irbp18 to terminal repeats of P element transposons (Francis et al.
127 2016). The Xrp1/Irbp18 heterodimer acts as a sequence-specific transcription factor
128 (Kiparaki et al. 2022). In *Rp*$^{+/-}$ mutant cells, *Xrp1* and *irbp18* transcriptionally autoregulate,
129 which is needed for their expression and is essential for cell competition (Baillon et al.
130 2018; Blanco, Cooper, and Baker 2020). Xrp1 is a rapidly-evolving gene without any clear
131 mammalian homolog, although Irbp18 is the *Drosophila* homolog of C/EBP proteins
132 (Blanco, Cooper, and Baker 2020). Xrp1 may be functionally related to DDIT3/CHOP, a
133 mammalian bZip protein with roles in the ER stress response, because DDIT3/CHOP
134 heterodimerizes with C/EBP, like Xrp1 does with Irbp18, because Xrp1 expression is also
135 induced by ER stress, and because overexpression of human DDIT3/CHOP in *Drosophila*
136 produces a phenotype resembling that of Xrp1 expression (Blanco, Cooper, and Baker
137 2020; Brown et al. 2021; Ochi et al. 2021).
138 Xrp1 was initially found as one of the most abundantly expressed transcriptional
139 targets of p53 following irradiation (Brodsky et al. 2004), and Xrp1 has also been proposed
140 to contribute genome integrity, because irradiation of Xrp1 mutant flies potentiates loss
141 of heterozygosity (Akdemir et al. 2007). Xrp1 may also contribute to DNA recombination,
142 since it promotes transposition of the *Drosophila* P elements, to which it also binds directly
143 (Francis et al. 2016).
144 We hypothesized that Xrp1 is an effector of p53 function in the *Drosophila* DDR,
145 and that by activating Xrp1 expression directly, ie by-passing p53, *Rp* mutant cells
146 activate a portion of what might otherwise be considered p53 responses, and that this
147 includes cell competition (Baker, Kiparaki, and Khan 2019). If this was correct, then Xrp1

148 should be required for aspects of the p53-dependent DDR, and p53 activity differences
149 should be able, through Xrp1, to trigger competition between cells, by-passing the
150 requirement for an *Rp* mutation. Here, we test these hypotheses. We confirm that Xrp1 is
151 upregulated by p53 and show that Xrp1 is needed for expression of multiple p53 target
152 genes, contributing to p53-dependent apoptosis in response to irradiation. We show that
153 differential activation of p53 does indeed cause cell competition in *Drosophila*, as it does
154 in mammals. Unexpectedly, however, the mechanism of p53-driven cell competition was
155 not Xrp1-dependent. On the contrary, Xrp1 suppressed the expansion of $p53^{-/-}$ mutant cell
156 clones experiencing genotoxic stress. Our work then revealed roles of both Xrp1 and p53
157 in limiting the accumulation of damaged and aneuploid cells. This suggests that it is cells
158 with genomic alterations resulting from DNA damage that are behind the super-
159 competitive behavior of *p53* mutant cells, which is enhanced in the absence of Xrp1
160 because of the p53-independent role of Xrp1 in eliminating aneuploid cells. Our work
161 indicates that the connection between p53 and cell competition seen in mammals is
162 shared in *Drosophila*. Additionally, it highlights the importance of cell competition as a
163 mechanism containing genomic instability by eliminating aneuploid cells, and suggests
164 that under some conditions, aneuploid cells that evade cell competition themselves
165 become super-competitors.
166
167 RESULTS
168 **DNA damage induced expression of Xrp1**
169 Xrp1 mRNA is upregulated by p53 within 30 mins of irradiation of *Drosophila*
170 embryos (Brodsky et al. 2004; Akdemir et al. 2007), perhaps by direct binding of the p53
171 within Xrp1 locus (Kurtz et al. 2019). To confirm that Xrp1 is a p53 target in imaginal
172 discs, we explored Xrp1 expression in third instar larval wing discs using a fly line
173 expressing Xrp1 protein with a C-terminal HA tag, encoded at the endogenous locus
174 (Blanco, Cooper, and Baker 2020). Wild type wing discs exhibited few Xrp1-HA positive
175 cells; these might reflect spontaneous DNA damage or another cellular stress (Figure 1A).
176 Exposure to 1500 Rads of γ-rays (IR) induced strong Xrp1-HA positive cells by 2h after
177 IR, which further increased by 4h after IR (Figure 1B-C). DNA damage induced Xrp1-HA
178 expression was non-uniform, with some cells showing higher expression levels than
179 others, which was different from the more uniform Xrp1-HA expression seen in $Rp^{+/-}$

180 mutant wing discs (Figure 1D). A similar, salt-and-pepper pattern of Xrp1 was observed
181 with Xrp1 antibody (Figure 1E and F). The specificity of Xrp1-HA expression was further
182 confirmed by its reduction after RNAi for Xrp1(Figure 1G).
183 Next, we tested the requirement of p53, using a dominant-negative form of p53
184 encoded by *UAS-p53*^{H159N}. This was expressed in posterior wing compartments, so that
185 Xrp1-HA expression levels could be compared to anterior compartments of the same
186 wing discs that lacked dominant-negative p53 expression. Dominant-negative p53
187 significantly reduced IR-induced Xrp1-HA (Figure 1H), as previously reported for Xrp1
188 transcription in irradiated embryos (Brodsky et al. 2004; Akdemir et al. 2007). Imaginal
189 disc Xrp1 was also p53-dependent at the transcript level, with a ~3x reduction in mRNA
190 level seen after qRT-PCR from irradiated *p53*$^{-/-}$ wing discs (Figure 1- figure supplement
191 1A).
192 Interestingly, Xrp1-HA protein expression was only slightly affected by Irbp18
193 knock-down (Figure 1I), arguing that autoregulation contributes little to IR-induced *Xrp1*
194 transcription. Consistent with this, 50% of the normal *Xrp1* mRNA level remained in the
195 *Xrp1*$^{m2-73}$/*Df* mutant background, in accordance with continued transcription of the
196 functionally null *Xrp1*$^{m2-73}$ point mutant allele (Figure 1- figure supplement 1A). This was
197 different from Xrp1 expression in *Rp*$^{+/-}$ mutants, where Xrp1 autoregulation is important
198 (Baillon et al. 2018; Blanco, Cooper, and Baker 2020). The expression of the Xrp1-LacZ
199 enhancer trap, a reporter upregulated in *Rp*$^{+/-}$ mutants (Baillon et al. 2018; Lee et al. 2018),
200 was also moderately elevated after irradiation (Figure 1J, K). Xrp1-LacZ expression,
201 however, depended on Xrp1 and Irbp18 function, both after irradiation and in the
202 unirradiated control (Figure 1- figure supplement 1B-E). Unexpectedly, reduced p53
203 function slightly elevated the expression of Xrp1-LacZ expression after irradiation,
204 instead of reducing it (Figure 1L). The discordance between regulation of Xrp1-LacZ
205 expression with that of Xrp1 mRNA and Xrp1-HA protein suggests that Xrp1-LacZ
206 differs from endogenous Xrp1 regulation, either at the transcriptional or post-
207 transcriptional levels.
208
209 **Regulation of p53-dependent DDR target genes by Xrp1**
210 It is known from mammalian studies that p53 regulates a complex transcriptional
211 program of hundreds or even thousands of genes (Levine, Hu, and Feng 2006). However,
212 depending on the study, only 122-346 p53-dependent genes have a p53 consensus motif

213 in the promoter or upstream region, suggesting that they could be direct p53 targets (Wei
214 et al. 2006; Fischer 2017). It is thought that p53 directly controls context-specific, core
215 transcription programs that in turn regulate further secondary, indirect targets (Andrysik
216 et al. 2017). Since Xrp1 is a transcription factor and a p53 target in *Drosophila*, Xrp1 is a
217 candidate to bring secondary target genes under the indirect control of p53. Accordingly,
218 when we compared p53-dependent genes in the DDR (Brodsky et al. 2004; Akdemir et al.
219 2007) with Xrp1-dependent genes in $Rp^{+/-}$ wing imaginal discs (Lee et al. 2018) and Xrp1-
220 dependent genes in wing imaginal discs over-expressing Xrp1 (Baillon et al. 2018). We
221 found 21 of 42 Rapidly Induced p53-target genes (RIPD) were Xrp1-regulated in wing
222 discs (Figure 2A). These genes were associated with Gene Ontology (GO) terms
223 transcription factors, cell death, DNA repair, and redox response (Figure 2B).

224 To test if Xrp1 was needed for regulating the DNA damage induced targets of p53,
225 we employed available reporter lines and also confirmed gene expression by qRT-PCR.
226 *GstD-lacZ* is a redox response reporter that is induced in response to oxidative stress
227 (Sykiotis and Bohmann 2008), and is elevated in $Rp^{+/-}$ wing discs downstream to Xrp1 (Ji
228 et al. 2021; Kiparaki et al. 2022). *GstD-lacZ* was expressed in response to IR, dependent on
229 p53 (Figure2C-D). We found that Xrp1 and Irbp18 were needed for p53-dependent
230 expression of *GstD-lacZ* after IR (Figure 2F-G). This was also in accordance with Xrp1
231 binding sites being present in the *GstD*-lacZ reporter (Brown et al. 2021). To confirm that
232 antioxidant genes themselves were affected like the *GstD-lacZ* reporter was, we measured
233 *GstD1* mRNA levels in wing discs. Induction of *GstD1* mRNA by IR indeed depended on
234 both p53 and Xrp1 (Figure 2M).

235 Another stress pathway activated in DDR is the Jun Kinase pathway (Picco and
236 Pages 2013). JunK activity is also Xrp1-dependent in $Rp^{+/-}$ wing discs (Lee et al. 2018; Ji et
237 al. 2019). We found the JNK reporter *TRE-dsRed* was induced by IR in a p53-dependent
238 manner (Figure 2H-J), and was also Xrp1/Irbp18 dependent (Figure 2K & L). The TNF-
239 alpha ligand *eiger (egr)* has been proposed to activate JNK signaling in the DDR (Sanchez
240 et al. 2019). Surprisingly, however, *egr* transcription was p53-dependent but independent
241 of Xrp1, which questions whether it is solely responsible for JNK signaling in the DDR
242 (Fig. 2N).

243 All except one of the p53-dependent DNA repair genes induced in DDR were also
244 potential Xrp1 targets (Figure 2B). We looked at wing disc mRNA levels of representative
245 genes from the major DNA repair pathways. These were the homologous recombination

246 pathway gene *rad50*, the translesion polymerase DNA polymerase zeta subunit 1, *mus205*,
247 and Non-Homologous End Joining (NHEJ) pathway genes DNA ligase 4 (*lig4*) and *Ku80*.
248 We found that IR-dependent expression of all these genes depended on Xrp1 at least as
249 strongly as upon p53 (Figure 2O-R). A well-known aspect of DDR is apoptotic death of
250 severely damaged cells, dependent in *Drosophila* on p53-dependent induction of the pro-
251 apoptotic genes *rpr* and *hid* (Brodsky et al. 2004; Dekanty, Barrio, and Milán 2015). To
252 explore the potential role of Xrp1, we examined reporter lines for *rpr* and *hid*, which are
253 expressed in response to IR and are widely used as p53 reporters (Brodsky et al. 2000;
254 Tanaka-Matakatsu et al. 2009; Fan et al. 2010). Two reporter lines for *hid* are the *hid5′F-*
255 *wt-EGFP* reporter, which contains ~2 kb spanning the *hid* promoter from +16 to −2210bp
256 relative to the transcription start site, and the $hid^{20\text{-}10}$-*lacZ* reporter, which contains a
257 distinct 10 kb sequence from the *hid* upstream region (Tanaka-Matakatsu et al. 2009; Fan
258 et al. 2010) (Figure 3A). As expected, *hid5′F-wt-EGFP* was highly induced after IR (Figure
259 3B-C), and was p53-dependent (Figure 3D). Both *Xrp1* and *Irbp18* RNAi also reduced the
260 *hid5′F-wt-EGFP* expression to the same extent as p53 dominant-negative did (Figure 3E-
261 F). The $hid^{20\text{-}10}$-*lacZ* reporter was also induced by IR and was dependent upon p53 (Figure
262 3G-I). Both *Xrp1* and *Irbp18* RNAi reduced IR-dependent $hid^{20\text{-}10}$-*lacZ* expression, although
263 not so much as p53 dominant-negative (Figure 3J-K). We assessed *rpr* expression using
264 the rpr^{150}-*lacZ* reporter, containing a 150bp sequence including a putative p53 binding site
265 ~4.8kb upstream of the *rpr* gene (Brodsky et al. 2000). In controls, rpr^{150}-*lacZ* reporter
266 exhibits uniform expression in most of the wing disc, on which is superimposed a region
267 of elevated expression bordering the posterior wing pouch and notum region (Alpar,
268 Bergantiños, and Johnston 2018; Li et al. 2020) and (Figure 3L). Because IR enhanced all
269 aspects of rpr^{150}-*lacZ* expression (Figure 3L,M and Figure 3- Supplemental 1A), we
270 measured the average rpr^{150}-*lacZ* expression level in anterior and posterior compartments
271 and computed the ratio of posterior-to-anterior expression level as a readout of genetic
272 perturbations applied to the posterior compartments (Figure 3- Supplemental 1B). The
273 increase in rpr^{150}-*lacZ* following IR was p53-dependent, as expected, but unaffected by
274 RNAi for either Xrp1 or Irbp18 (Figure 3N-P- Supplemental 1B).

275 To confirm that these studies of *hid* and *rpr* reporters were indeed reflective of the
276 expression of the genes themselves, mRNA levels were measured in wing discs after IR.
277 Consistent with the reporter studies, induction of *hid* mRNA by irradiation was
278 completely dependent on p53, and partially dependent on Xrp1 (Figure 3Q). Induction of

rpr mRNA expression was completely dependent on p53 but was unaffected by the loss of Xrp1(Figure 3R).

Taken together, these results strongly support the notion that p53 target genes identified through the *Drosophila* DDR include secondary targets that are more directly induced by the p53-dependent expression of Xrp1. Only two p53 target genes, *egr* and *rpr*, were induced independently of Xrp1 out of the nine examined, although *hid* induction has both Xrp1-dependent and -independent components. Analysis of p53 and Xrp1 binding motifs supported this conclusion. Sequences matching the p53 binding consensus has been located within both the rpr^{150}-*lacZ* reporter and the *hid5'F-wt-EGFP* reporter (Brodsky et al. 2000; Wichmann, Uyetake, and Su 2010). Consensus binding sites for the Xrp1/Irbp18 heterodimer have been determined by bacterial one-hybrid studies (Fly Factor Survey) (Zhu et al. 2010) and from ChIP-seq after Xrp1 over-expression in larval wing disc (Baillon et al. 2018). Such sequences are footprinted by Xrp1/Irbp18 in the P element terminal repeat, (Francis et al. 2016), and sufficient to confer Xrp1/Irbp18-dependent transcription on luciferase reporters (Kiparaki et al. 2022). Using an *in-silico* motif finder (INSECT) (Rohr et al. 2013), we found three Xrp1/Irbp18 binding motifs in the *hid5'F-wt-EGFP* reporter sequence and two in the $hid^{20\text{-}10}$-*lacZ* reporter sequence (Figure 3T), but we found none in the rpr^{150}-*lacZ* reporter that was expressed independently of Xrp1 and Irbp18 (Figure 3T). We conclude that, while *rpr* could be a direct target of p53 in the DDR, *hid* expression is partially dependent on Xrp1 induction downstream of p53, and the *hid5'F-wt-EGFP* reporter entirely so.

Xrp1 is sufficient for the expression of p53- dependent DDR target genes

It is possible that Xrp1 might activate p53 to create positive feedback in the DDR. We used the rpr^{150}-*lacZ* reporter, which is activated by p53 but not Xrp1, to test how p53 activity was affected by Xrp1 over-expression. As expected, Xrp1 overexpression in the wing pouch resulted in huge amount of cell death (Figure 4- figure supplement 1A-B), but no discernable increase in rpr^{150}-*lacZ* levels (Figure 4- figure supplement 1C-D). Similar results were obtained by expressing Xrp1 in the differentiating eye discs (Fig. 4A-B). Thus, Xrp1 does not seem to cause p53 activation, but to act downstream of p53.

Next, we tested if Xrp1 was sufficient for the expression of target genes. We found that Xrp1 overexpression in the eye disc led to a robust upregulation of $hid^{20\text{-}10}$-*lacZ* (Figure 4 C and D) and *hid5'F-wt-EGFP* (Figure 4E and F). Xrp1 also regulates JNK and

312 oxidative stress responses after DNA damage, and Xrp1 overexpression was sufficient to
313 activate reporters for these cellular pathways. Levels of both *JNK-dsRED* and *GstD-lacZ*
314 were highly upregulated by Xrp1 (Figure 4- figure supplement 1E and F & G and H).
315 These results support the idea that Xrp1 functions downstream of p53, and is sufficient
316 for the expression of a subset of p53- dependent genes.
317
318 **Xrp1 contributes to DNA damage induced cell death**
319 To see whether the regulation of cell death genes by Xrp1 was functionally
320 significant, the *p53*-dependent apoptosis that occurs in response to irradiation was
321 examined. Cell death begins within 30 minutes after IR treatment and is completely
322 dependent on p53 until 4-5 hours later (Wichmann, Jaklevic, and Su 2006; McNamee and
323 Brodsky 2009). Accordingly, p53 dominant-negative expression in posterior
324 compartments substantially reduced the IR-induced cell death, leaving of only a few cells
325 positive for the activated Dcp-1 caspase (Figure 5B & D). Xrp1 RNAi (two independent
326 lines) and Irbp18 RNAi both reduced cell death in the posterior compartment (Figure 5C
327 & D), to a lesser extent than p53 dominant-negative did.
328 We also examined the cell-autonomy of p53 and Xrp1 function using clones of
329 mutant cells. Wild type and $p53^{+/-}$ heterozygous cells exhibited similar cell death levels
330 after irradiation, but cell death was absent from $p53^{-/-}$ null clones (Figure 5F,H). There
331 was little cell death observed in $Xrp1^{+/-}$ (heterozygous) and $Xrp1^{-/-}$ (null) tissue as opposed
332 to high amount of cell death observed in $Xrp1^{+/+}$ (wild type twin spot) (Figure 5G,H)
333 (effects of Xrp1 mutation on *Rp* mutant cells are also dominant through
334 haploinsufficiency) (Lee et al. 2018). Control clones had no effect on IR-induced cell death
335 (Figure 5E,H).
336 Taken together, these results show that Xrp1 contributes to p53-mediated cell
337 death in response to irradiation, although this is partial because p53 also regulates cell
338 death genes directly such as *rpr* (Figure 3R). We also tested the contribution of Xrp1 to
339 effects of p53 over-expression. Over-expression of p53 in the developing eye causes a
340 rough eye phenotype in adults (Figure 5- Supplemental figure 1A (Ollmann et al. 2000;
341 Jin et al. 2000). Xrp1 knock-down very slightly reduced the rough eye phenotype, unlike
342 dominant-negative p53, which rescued completely (Figure 5- figure supplement 1B,C).
343 p53 over-expression in wing discs resulted in massive cell death that was reduced only
344 weekly by Xrp1 knock-down or mutant genotypes (Figure 5- figure supplement 1D -H).

345 This partial dependence on Xrp1 may reflect the observation that p53 over-expression led
346 to rather little Xrp1 protein expression (Figure 5 figure supplement 1I), which is a
347 difference from endogenous p53 activity in the DDR, suggesting that IR induced (Figure
348 1H) and over-expressed p53 mechanisms may not be identical.
349
350 **Differential activation of p53 triggers cell competition in *Drosophila***
351 Differences in p53 activity between mammalian cells often result in cell
352 competition (Bondar and Medzhitov 2010; Wagstaff et al. 2016; Zhang et al. 2017). In
353 *Drosophila*, p53 is dispensable for the elimination of $Rp^{+/-}$ cells (Kale et al. 2015; Lee et al.
354 2018), and cells with and without the p53 gene do not compete with one another (de La
355 Cova et al. 2014). If Xrp1 is a downstream effector of *Drosophila* p53, however, and
356 differences in Xrp1 activity lead to cell competition, then we hypothesized that
357 differences in p53 activity between cells might lead to competition, in *Drosophila* as in
358 mammals.
359 To test this hypothesis, we developed a strategy for chronic mild activation of p53
360 by feeding the genotoxic drug Cisplatin (Cis-Pt). Cis-Pt causes p53 activation through
361 double-strand breaks and other DNA damage (Dasari and Tchounwou 2014). Since
362 feeding with 0.5-1mM Cis-Pt produce high levels of DNA damage and cell death even in
363 non-mosaics (Figure 6 Supplement 1A) (Khan et al. 2017), we modified this protocol by
364 reducing Cis-Pt dosage. Third instar larvae fed with 0.01 mM or 0.02 mM Cis-Pt (starting
365 at 48h after egg laying) exhibited negligible cell death or DNA damage, as measured by
366 anti-active Dcp1 or anti γH2Av, and only a few Dcp-1 positive cells were seen after
367 feeding 0.05mM Cis-Pt (Figure 6 figure supplement 1A). Anti-γH2Av detects histone
368 H2Av phosphorylated at ser-237 and is a marker for double-strand breaks (Madigan,
369 Chotkowski, and Glaser 2002). We used 0.05 mM Cis-Pt feeding for subsequent
370 experiments, although some results were also corroborated using 0.02 mM Cis-Pt.
371 Neither concentration caused adult defects such as notched wing margins that are seen
372 after more severe DNA damage (Wells and Johnston 2012), although there was a
373 pupariation delay of ~12h or ~ 24h associated with 0.02 mM and 0.05 mM Cis-Pt
374 respectively, and 0.05mM Cis-Pt led to some arrest of development at the pharate pupa
375 stage. We then used FRT mediated somatic recombination in *p53* heterozygotes to
376 generate reciprocal clones of $p53^{-/-}$ and $p53^{+/+}$ cells, with Cis-Pt fed from the time of clone

377 induction, leading to clones of cells with and without p53 activity that had been exposed
378 to mild genotoxic stress (Figure. 6A & see methods).
379 The p53 reporter *rpr*^{150}-lacZ was elevated by 0.05 mM Cis-Pt diet (Figure. 6B, C).
380 In the absence of Cis-Pt, the ratio of *p53*$^{-/-}$ and *p53*$^{+/+}$ clone sizes was similar to controls, as
381 reported previously (Figure. 6D, E, H) (de La Cova et al. 2014). By contrast, in the presence
382 of Cis-Pt the ratio of *p53*$^{-/-}$ clone size to sister *p53*$^{+/+}$clone sizes was ~4 by 72 hours after
383 clone induction and ~ 6 at 96h after clonal induction, although Cis-Pt had little effect on
384 control clone sizes (Figure. 6F-H). Similar results were seen using 0.02mM Cis-Pt (Figure
385 6- figure supplement 1B-F). We confirmed these results in eye development, where
386 0.02mM Cis-Pt enhanced the contribution of *p53*$^{-/-}$ mutant clones to adult eyes (Figure 6
387 figure supplement 1G-J). We also compared absolute *p53*$^{-/-}$ clone sizes in the presence and
388 absence of Cis-Pt. This analysis revealed that *p53*$^{-/-}$ mutant clones grew ~ 2.5-fold bigger
389 in the presence of Cis-Pt (Figure 6I), whereas the reciprocal *p53*$^{+/+}$ sister clones grew ~2
390 fold smaller (Figure 6J).
391 These results were consistent with competition between clones of *p53*$^{+/+}$ cells
392 experiencing p53 activity and clones of *p53*$^{-/-}$ cells, but they also could be explained by a
393 cell-autonomous p53-dependent growth retardation in the presence of Cis-Pt. To
394 distinguish these possibilities, we performed a 'neutral-clone assay' that compared the
395 growth of *p53*$^{+/+}$ clones adjacent to *p53*$^{-/-}$ sister clones with the growth of independent,
396 spatially uncorrelated clones within the same wing discs, derived from simultaneous
397 mitotic recombination of a distinct chromosome. In the absence of Cis-Pt, the two
398 independent categories of clone, one the sisters of *p53*$^{-/-}$ clones and one the sisters of *p53*$^{+/+}$
399 clones, were both indistinguishable in size. By contrast, in the presence of 0.05 mM Cis-
400 Pt, the clones with *p53*$^{-/-}$ sisters were ~4-fold smaller than the clones with *p53*$^{+/+}$ sisters
401 (Figure 6K-M). These results show that the growth disadvantage of clones of wild type
402 cells with *p53*$^{-/-}$ sisters after Cis-Pt exposure is not a cell-autonomous effect of p53 activity,
403 but is a property only of wild type clones with nearby *p53*$^{-/-}$ sister clones. This indicates
404 that differences in p53 activity lead to cell competition in *Drosophila* imaginal discs, as
405 they do in many mammalian tissues, and that *p53*$^{-/-}$ cells out-compete nearby cells in
406 which *p53* is active, even when the p53 activity is mild compared to that usually studied
407 as representative of the DDR.
408 We asked if the growth disadvantage *p53*$^{+/+}$ clones with *p53*$^{-/-}$ sister clones was due
409 to more robust DNA damage signaling than the *p53*$^{-/-}$ mutant cells. We saw no difference

410 in γH2Av staining between *p53*$^{-/-}$ mutant clones and their *p53*$^{+/+}$ sisters in the absence of
411 Cis-Pt (Figure 6- figure supplement 2A-B). There was no significant change after Cis-Pt
412 feeding, indicating that Cis-Pt causes only low levels of DNA damage that do not
413 accumulate substantially in *p53*$^{-/-}$ mutant cells (Figure 6- figure supplement 2E-H). By
414 contrast, irradiation with 1500 Rads of γ-rays gave rise to significantly higher γH2Av
415 levels, that were still further elevated in *p53*$^{-/-}$ mutant clones compared to their *p53*$^{+/+}$ sister
416 clones (Figure 6- figure supplement 2D-C). This accumulation of *p53*$^{-/-}$ mutant cells with
417 DNA damage might be due to lack of apoptosis of such cells in the wing disc any such
418 effect of 0.05mM Cis-Pt must be significantly smaller.
419
420 **p53-mediated cell competition independent of Xrp1**
421 Since Xrp1 is downstream of p53 in the DDR, we hypothesized that it could be
422 higher Xrp1 that results in cell competition of wild type cells growing next to *p53*$^{-/-}$ mutant
423 cells. To test this, we first examined the effect of Cis-Pt on Xrp1 mutant cells. Although
424 *Xrp1*$^{-/-}$ mutant clones grew like their *Xrp1*$^{+/+}$ sister clones in the absence of Cis-Pt, as
425 reported previously Figure 7(A, E) (Baillon et al. 2018; Lee et al. 2018), Cis-Pt exposure
426 led to larger *Xrp1*$^{-/-}$ mutant clones and smaller *Xrp1*$^{+/+}$ twin-spots (Figure 7B, D, E). We
427 also observed that *irbp18*$^{-/-}$ mutant clones grew larger than their *irbp18*$^{+/+}$ sister clones in
428 the presence of Cis-Pt, suggesting that the Xrp1/Irbp18 heterodimer was activated by
429 Cis-Pt (Figure 7G- I). Thus, Cis-Pt has similar effects on clones of *Xrp1* and *p53* mutant
430 cells, consistent with both genes functioning in the same pathway.
431 To test whether Xrp1 was the downstream effector of p53 in cell competition, we
432 explored whether different levels of p53 activity could lead to cell competition in the
433 absence of Xrp1. We depleted posterior compartments of Xrp1 by RNAi and examined
434 competition between *p53*$^{-/-}$ mutant clones and their *p53*$^{+/+}$ twin-spots. In the absence of
435 Cis-Pt, the ratio of *p53*$^{-/-}$ and *p53*$^{+/+}$ clone sizes was comparable in the anterior and the
436 posterior compartments, indicating that it was not affected by Xrp1 (Figure 8A-C). If Xrp1
437 was required for competition between cells with different p53 activities, we expected that
438 *p53*$^{-/-}$ and *p53*$^{+/+}$ clone sizes would remain similar in Xrp1-depleted posterior
439 compartments in the presence of Cis-Pt. Contrary to this expectation, *p53*$^{-/-}$ clones were
440 larger than *p53*$^{+/+}$ twin spots when Xrp1 was depleted in the presence of Cis-Pt, just as
441 they had been without Xrp1 depletion (Figure 8D-F). To analyze this in more detail, we

442 compared the clone sizes of all the genotypes. We found that, in the absence of Cis-Pt,
443 growth of all the *p53*$^{-/-}$ and *p53*$^{+/+}$ clones was equivalent, regardless of *Xrp1* knockdown,
444 confirming earlier results (Figure 6E,H). In the presence of Cis-Pt, all the *p53*$^{-/-}$ clones grew
445 larger and all the *p53*$^{+/+}$ clones grew less, also confirming earlier experiments (Figure
446 6G,H). Neither of these Cis-Pt effects was reversed by Xrp1 knockdown (Figure 8D-F). In
447 fact, in the presence of Cis-Pt, the *p53*$^{-/-}$ clones depleted for Xrp1 grew significantly larger
448 than plain *p53*$^{-/-}$ clones in the presence of Cis-Pt (Figure 8G). In addition, the adjacent
449 *p53*$^{+/+}$ sister clones depleted for Xrp1 grew less than *p53*$^{+/+}$ sister clones able to express
450 Xrp1, although this difference was not statistically significant after correction for multiple
451 testing (Figure 8H).
452 These results were not consistent with our original hypothesis that Xrp1 mediates
453 the competitive elimination of cells with higher p53 activity, because the p53-dependent
454 growth reduction of wild type clones under genotoxic stress and near to *p53*$^{-/-}$ clones
455 occurred independently of Xrp1. In addition, *p53*$^{-/-}$ clones exposed to Cis-Pt grew even
456 more when Xrp1 was depleted, indicating an unexpected, p53-independent function of
457 Xrp1 under genotoxic stress.
458
459 **Xrp1 function in mediating competitive cell death to limit genomic instability**
460 If Xrp1 was activated through p53, we would not expect Xrp1 expression or
461 function in *p53*$^{-/-}$ cells exposed to Cis-Pt. Instead, we observed a salt-and pepper Xrp1
462 expression pattern after Cis-Pt exposure that included *p53*$^{-/-}$, *p53*$^{+/-}$, and *p53*$^{+/+}$ cells (Figure
463 8- figure supplement 1A,B). This expression was much lower than seen after 1500 Rads
464 of IR. By contrast, Cis-Pt-treated wing discs containing *Xrp1* clones showed Xrp1
465 expression only in *Xrp1*$^{+/+}$ cells, not *Xrp1*$^{+/-}$ cells or *Xrp1*$^{-/-}$ cells (Figure 8- figure
466 supplement 1C). These results were unexpected, because previously we had found that
467 p53 was required for DNA damage to induce Xrp1 expression (Figure 1H and Figure 1-
468 figure supplement 1A). Using Xrp1-HA to monitor Xrp1 expression, and enGal4 to
469 express dominant-negative p53 in posterior compartments, we confirmed the salt-and-
470 pepper pattern of Xrp1 expression after Cis-Pt treatment, and, surprisingly, found Xrp1-
471 HA expression was increased where p53 was inhibited, not reduced (Figure 8
472 supplement 1D-G). We also noticed that Xrp1 expression typically occurred in small cell
473 clusters, possibly clonal.

474 Notably, we have previously described p53-independent induction of Xrp1 in
475 wing discs in response to IR (Ji et al. 2021). Unlike p53-dependent Xrp1 expression in the
476 acute DDR, which occurs within 2-4h, p53-independent induction peaks 16-24h after
477 irradiation. This Xrp1 expression is thought to occur in aneuploid and segmental-
478 aneuploid cells that arise following DNA damage (McNamee and Brodsky 2009; Ji et al.
479 2021). More than half of this expression depends on RpS12, which is also required for
480 Xrp1 expression in $Rp^{+/-}$ cells (Lee et al. 2018; Ji et al. 2019; 2021). Here, we verified that
481 Xrp1-HA was expressed in scattered cells 24h following irradiation (Figure 8 supplement
482 1H,I). Xrp1-HA expression was completely eliminated by knock-down of Xrp1, but not
483 by knock-down of Irbp18 (Figure 8 supplement 1J,K). Like the results with Cis-Pt,
484 however, 24h post-irradiation Xrp1-HA expression was enhanced several-fold by p53
485 inhibition (Figure 8 supplement 1 L, N). Like Xrp1 expression in aneuploid cells, p53-
486 independent Xrp1 expression was significantly reduced in the RpS12 mutant background
487 (Figure 8M,N). These results are consistent with the notion that, following irradiation or
488 Cis-Pt feeding, the p53-dependent DDR suppresses the acquisition of aneuploidy, and
489 that if p53 is inhibited then an increased frequency of aneuploid cells results, and these
490 cells express Xrp1 in an RpS12-dependent manner. Xrp1 activity would then be expected
491 to remove these cells by cell competition.

492 To explore the impact of p53 on genome integrity and Xrp1 activity further, we
493 looked at IR-induced DNA damage using anti-γH2Av. Consistent with previous results,
494 24h after irradiation most acute DNA damage has been repaired although a limited
495 amount remains, along with some continuing cell death (Figure 9A) (Wichmann, Jaklevic,
496 and Su 2006; McNamee and Brodsky 2009). A portion of the cell death continues in the
497 absence of p53 (Wichmann, Jaklevic, and Su 2006; McNamee and Brodsky 2009).
498 Consistent with the conclusion that this includes competitive death of aneuploid cells
499 (McNamee and Brodsky 2009; Ji et al. 2021), we found that the p53-independent cell death
500 was substantially reduced by Xrp1 knockdown (Figure 9C,D). Anti-γH2Av labeling 24h
501 after irradiation was greatly increased in the absence of p53, indicating persistence of
502 DNA damage (Figure 9B). Anti-γH2Av labeling was even further increased after Xrp1
503 knockdown in the absence of p53, showing that Xrp1 contributes to the elimination of
504 cells with DNA damage even in the absence of p53, presumably through cell competition
505 that removes aneuploid cells. Consistent with this hypothesis, Xrp1 expression was

506 induced in a subset of the damaged cells that persisted when p53 was inhibited (Figure
507 9E,F).
508 To assess the effect of aneuploidy, the effect of Cis-Pt on clones of *rpS12* mutant
509 cells was examined. Whereas the cell competition-defective *rpS12*^{G97D} allele has no effect
510 on clone growth in the wing disc in the absence of DNA damage (Figure 9 supplement 1
511 A-C) (Kale et al. 2018), *rpS12*$^{G97D/G97D}$ clones overgrew their *rpS12*$^{+/+}$ twin-spots in the
512 presence of Cis-Pt (Figure 9 supplement 1 A-C), although the effect was smaller than that
513 seen for p53 or Xrp1 mutants. Importantly, although RpS12 is implicated in the
514 competitive removal of *Rp* mutant and aneuploid cells, it did not affect cell death in the
515 acute DDR 2h after IR, suggesting that Xrp1 function in acute DDR depends on p53 not
516 RpS12 (Figure 9 supplement 1D-F). These results are consistent with previous
517 conclusions that Xrp1 expression can be induced by at least two independent pathways,
518 by p53 in the acute DDR, and by RpS12 in the competitive elimination of *Rp*$^{+/-}$ cells and
519 of aneuploid cells monosomic for one or more *Rp* gene loci, that latter typically occurring
520 ~24h after acute DNA damage (Lee et al. 2018; Ji et al. 2021). Both mechanisms need to be
521 considered to fully account for Xrp1 requirements in the presence of Cis-Pt.
522
523 DISCUSSION
524 *Drosophila* p53 shows sequence similarity and conserved overall structure with
525 human p53, and is the key effector of the DDR in *Drosophila* as well as in mammals
526 (Brodsky et al. 2000; Ollmann et al. 2000). There are some differences: in mammals, for
527 example, DNA damage results in cell cycle (G1 and G2/M) arrest due to p53-dependent
528 transcriptional activation of p21 and other targets 14-3-3σ and mir34a (Chen 2016),
529 whereas cell cycle arrest in the *Drosophila* DDR is mediated by *grps*/*Chk1* and *mnk*/*Chk2*,
530 independently of p53 (Brodsky et al. 2004). So far, *Drosophila* p53 has not been shown to
531 be important for eliminating cells by competition, which is clearly a function of p53 in
532 mammals (Baker 2020). Cell competition of multiple *Drosophila* genotypes, including the
533 *Rp*$^{+/-}$ genotype where cell competition was first described, depends on the transcription
534 factor Xrp1 (Lee et al. 2016; 2018; Baillon et al. 2018; Langton et al. 2021; Ochi et al. 2021;
535 Kiparaki et al. 2022). Xrp1 is also a target of p53 in the acute DDR, suggesting that Xrp1
536 could mediate a relationship between p53 and cell competition in *Drosophila* (Baker,
537 Kiparaki, and Khan 2019). In this work, we establish that Xrp1 is a major effector of p53

538 in the *Drosophila* DDR, and we show that differences in p53 activity cause cell competition
539 in *Drosophila*, as in mammals. Xrp1 retards the competitive expansion of *p53*$^{-/-}$ mutant
540 cells, however, through its p53-independent role in limiting accumulation of aneuploid
541 cells. This correlates with a role of Xrp1 in preventing accumulation of damaged cells in
542 *p53*$^{-/-}$ mutant clones under genotoxic stress, suggesting that it is these damaged cells that
543 are responsible for cell competition. Our results and conclusions are summarized in
544 Figure 10.
545
546 **Xrp1 is an effector of p53 functions in the DDR**
547 We show that, in imaginal discs, Xrp1 is induced downstream of p53 in the acute
548 phase of DDR at both RNA and protein levels (Figure 1). Unlike Xrp1 induction in *Rp*$^{+/-}$
549 cells, Xrp1 expression in the DDR occurs independently of autoregulatory transcription,
550 which may be why the Xrp1-LacZ enhancer trap shows less upregulation than the
551 endogenous transcript and protein. Multiple p53-dependent DDR genes, the majority in
552 our study, were Xrp1-dependent, including the pro-apoptotic gene *hid*. Even though *hid*-
553 reporters have been used as readouts of p53 activity (Fan et al. 2010; Zhang et al. 2014;
554 Ruiz-Losada et al. 2021; Chakravarti et al. 2022), they may be more accurately described
555 as targets of Xrp1. Other Xrp1 targets include DNA repair genes, GstD1, and Jun-kinase
556 signaling. Accordingly, Xrp1 is functionally required in the DDR, and in the absence of
557 Xrp1 DNA damage-induced cell death is reduced, although not eliminated, perhaps
558 because the pro-apoptotic gene *rpr* seems to be a direct target of p53 that does not require
559 Xrp1.
560 So far, integrating data from gene expression studies, binding motif and ChIP-Seq
561 searches, and global run-on sequencing of nascent mRNA has not yielded a consensus
562 on the core set of direct p53 target genes in mammals (Riley et al. 2008; Allen et al. 2014;
563 Fischer 2017). It is plausible that, as in *Drosophila*, mammalian p53 acts as a master
564 transcription factor that regulates a network of gene expression responses both directly
565 and also through intermediate transcription factors.
566
567 **Cell competition due to differential p53 activity**
568 If Xrp1 is activated and functions downstream of p53 in the DDR, we hypothesized
569 that differences in p53 activity between cells might lead to competition, as occurs between
570 cells with different Xrp1 levels in many examples of cell competition (Baker, Kiparaki,

571 and Khan 2019). To test this, we generated cells with chronic p53 activity by feeding the
572 genotoxic chemical Cis-Pt at concentrations that provoked p53 activity detectable with
573 the *rpr-LacZ* reporter but relatively little sign of acute DNA damage. Mutating p53 in
574 clones of cells then produced a situation where p53 activity was elevated in the wild type
575 cells compared to their p53-mutant neighbors. This clearly led to a competitive
576 disadvantage for wild type cells (Figure 6D-J). Clones of such cells showed diminished
577 growth in comparison to neutral clones of similar genotypes that did not have *p53*-mutant
578 sisters nearby (Figure 6K-M). Interestingly, the *p53*-mutant clones showed enhanced
579 growth, but our experiments did not permit us to distinguish whether this reflected the
580 absence of a cell-autonomous growth retardation that would normally result from p53
581 activity, or a non-autonomous stimulation due to out-competing nearby p53-wild type
582 cells.
583 These findings show that imaginal disc cells with higher p53 activity than their
584 neighbors suffer from cell competition with them, in *Drosophila* as in mammals. This has
585 not been recognized previously because *p53* mutant and wild type cells do not compete
586 in the absence of genotoxic stress, and because p53 is dispensable for the competitive
587 elimination of $Rp^{+/-}$ cells (Kale et al. 2015; de La Cova et al. 2004). $Rp^{+/-}$ cell competition is
588 independent of p53 because Xrp1 is induced in this genotype by RpS12, not p53 (Lee et
589 al. 2018). Given our present results, failure of wild type and *p53* mutant cells to compete
590 indicates that under normal conditions the baseline *p53* activity of imaginal disc cells is
591 below the threshold necessary for cell competition. Clonal expansion of *p53* mutant cells
592 in mammals indicates that this is not the case in mammalian tissues (Zhang et al. 2017).
593 The higher baseline p53 activity in mammals could reflect differences in p53 regulation
594 and turnover, but also could be caused simply by the much larger mammalian genome
595 providing a bigger target for spontaneous DNA damage. Many examples of mammalian
596 cell competition involving p53 activity also relate to genotoxic or mutant situations that
597 are expected to activate p53 (Nijhof et al. 2007; Bondar and Medzhitov 2010; Fernandez-
598 Antoran et al. 2019).
599
600 **p53 depleted cells accumulate damage and compete with their neighbors**
601 Our initial hypothesis was that, under chronic genotoxic stress, p53 would induce
602 Xrp1 expression through the DDR and that differences in Xrp1 expression would mediate
603 cell competition. Xrp1 expression was indeed induced by chronic Cis-Pt exposure.

604 Unexpectedly, however, Xrp1 expression also occurred independently of p53, and was
605 actually increased by p53 inhibition. Additionally, Xrp1 knock-down did not protect wild
606 type cells from competition with *p53* mutant cells under genotoxic stress, and may even
607 exacerbate it, while the overgrowth of *p53* mutant cells was potentiated by Xrp1-
608 depletion. These results were inconsistent with the idea of cell competition due to Xrp1
609 induction as part of the DDR, and indicate that Xrp1 in fact blunts an independent
610 pathway of cell competition in response to p53 differences. Below we suggest a plausible
611 explanation for these findings that is consistent with the available data.

612 One p53-independent route of Xrp1 expression is through RpS12. This occurs both
613 in $Rp^{+/-}$ cells and in cells with IR-induced genomic damage thought to change *Rp* gene
614 dose (Lee et al. 2018; Ji et al. 2021). Other mechanisms of Xrp1-induction, for example
615 following direct inhibition of translation factors, appear less dependent on RpS12
616 (Kiparaki et al. 2022). We showed here that Xrp1 expression in IR-damaged genomes was
617 also enhanced by p53 inhibition, and that this enhancement depended at least partially
618 on RpS12, the sensor of altered Rp gene dose. This suggests that, after irradiation, p53
619 function reduces the accumulation of cells with aneuploidy and other changes in genome
620 content that would induce Xrp1 expression through RpS12. We also found that p53
621 promoted the resolution of DNA damage and clearance of badly damaged cells following
622 irradiation, so that a great increase in cells with persistent unresolved DNA damage
623 resulted from irradiation when p53 was inhibited. The number of cells with unresolved
624 DNA damage is detectably increased further by inhibition of Xrp1 along with p53. Since
625 this represents a p53-independent role of Xrp1, it is more likely to represent failure to
626 eliminate cells with genome alterations by cell competition, rather than the role of Xrp1
627 in the DDR, because the latter is p53-dependent.

628 These studies of the response to IR now suggest a new hypothesis. Xrp1 expression
629 in imaginal discs exposed to Cis-Pt is not only due to a continuous DDR, mediated by
630 p53, but also occurs in sporadic cells where genotoxic stress has led to genome
631 rearrangements or aneuploidy, and hence to RpS12-dependent Xrp1 expression. This
632 could explain the salt-and-pepper Xrp1 expression pattern, and why Xrp1 expression in
633 the presence of Cis-Pt is enhanced by p53 inhibition. This notion is supported by the
634 finding that clones of cells homozygous for the cell competition-defective allele of *rpS12*
635 also have a growth advantage in the presence of Cis-Pt, like clones of cells mutant for *p53*
636 or *Xrp1* do.

637 Importantly, however, wild type cells exposed to Cis-Pt suffer a competitive
638 growth disadvantage in the vicinity of clones of *p53* mutant cells that is independent of
639 Xrp1. We suggest that this is related to the accumulation of DNA damage and genomic
640 alterations that we demonstrated occurs in cells exposed to genotoxic stress that are
641 unable to activate p53. Because this occurs even in the presence of wild type Xrp1, which
642 we show removes many cells damaged by irradiation, we suggest that *p53* mutant clones
643 contain cells with damaged genomes that cannot be recognized by the RpS12, Xrp1-
644 dependent cell competition pathway that predominantly recognizes *Rp* gene
645 haploinsufficiency. These could include cells with trisomies, or other increases in gene
646 content that are not characterized by *Rp* haploinsufficiency, or cells with genetic
647 alterations so substantial that they generate stress due to the mismatched levels of many
648 proteins, not only ribosomal proteins. Evidence for just such a stress was originally
649 observed in yeast strains with extra chromosomes, and has been demonstrated in
650 *Drosophila* imaginal discs by inhibition of spindle assembly checkpoint genes, which leads
651 to aneuploidy typically characterized by increased DNA content (Torres et al. 2007;
652 Dekanty et al. 2012; Joy et al. 2021). It is already known that such genotypes can be
653 growth-promoting and tumorigenic in *Drosophila* when cell death is prevented
654 (Clemente-Ruiz and Milán 2015). Our model is that such cells accumulate in p53-deficient
655 clones after genotoxic stress and exhibit enhanced growth and competitively inhibit
656 nearby wild type cells, an effect that is further enhanced by the absence of Xrp1, which
657 results in the accumulation of further damaged cells. In this model, differences in p53
658 activity do not lead to cell competition in *Drosophila* directly, but as a consequence of
659 different levels of genomic damage that arise in cells with and without p53 function.
660 It would be interesting to examine whether genome damage underlies examples
661 of p53-dependent cell competition observed in mammals. Our results, and model, are
662 consistent with the idea that p53 suppresses tumorigenesis in part by promoting cell
663 competition to remove abnormal cells, and that absence of p53 both abolishes this
664 protection and facilitates the accumulation of hyperplastic aneuploid cells that may
665 promote tumorigenesis.
666
667 ACKNOWLEDGEMENTS
668 We thank Drs. J. Secombe, M. Kiparaki, S. Nair, A. Kumar and S. Muliyil for
669 comments on the manuscript. Fly stocks were obtained from the Bloomington Drosophila

670 Stock Center (supported by NIH P40OD018537) and the Vienna Drosophila Resource
671 Center. Confocal microscopy was performed in the Analytical Imaging Facility of the
672 Albert Einstein College of Medicine (supported by the NCI P30CA013330) using the Leica
673 SP8 microscope acquired through NIH SIG 1S10 OD023591. The monoclonal antibody
674 mAb40-1a developed by J.R.Sanes was obtained from the Developmental Studies
675 Hybridoma Bank, created by the NICHD and maintained at the University of Iowa,
676 Department of Biology, Iowa City, IA 52242. This project was supported by grant
677 GM104213 from the National Institutes of Health.
678
679
680 MATERIAL AND METHODS
681 **1. Fly husbandry:**
682 Flies were raised at 25^0C on standard cornmeal and molasses medium, containing
683 the following ingredients per 1L: 18g yeast; 22g molasses; 80g malt extract; 9g agar; 65g
684 cornmeal; 2.3g methyl para-benzoic acid; 6.35ml propionic acid. Larvae were not
685 distinguished for their sex prior to dissection.
686
687 **2. DNA damage and genotoxic drug treatment:**
688 **γ-radiation:** Flies were grown in the standard cornmeal medium at 25^0C. After egg
689 laying was done for 24 hours, the flies were transferred to a fresh vial. Following this, the
690 larvae were allowed to grow until the wandering late III instar stage and DNA damage
691 was induced by treating them with γ-radiation from cesium-137 using a shepherd
692 irradiator. For most of the experiments, 1500 Rads were administered, and dissection was
693 performed at a specified time point after the irradiation.
694 **Cisplatin treatment:** Cisplatin dosage was calibrated to sub-lethal concentration
695 as explained in the results section. To avoid using large amount of cisplatin, we used a
696 smaller volume (2.5ml) of fly food. Fresh solution was made every day from powdered
697 Cisplatin by dissolving it in sterilized water at a concentration of 4mM (3mg in 250ml),
698 and it was serially diluted such that the final concentration of Cisplatin in the 2.5ml fly
699 food was 0.2mM or 0.05mM. The Cisplatin solution was added to the fly food by
700 micropipette, drop by drop, making sure it disperses throughout the food.
701

702 **3. Cell death and clone size quantification:**

703 **Cell death:** Cell death was quantified by counting number of Dcp-1 positive cells
704 with the help of ImageJ cell counter plugin. For UAS-Gal4 experiments Dcp-1 positive
705 cells in Gal4 to the control compartment was counted and compared as the ratio across
706 different genetic perturbations. In case of mutant wing discs, the number of Dcp-1
707 positive cell was counted in the entire disc and absolute number were compared.

708 **Clone size quantification:** Clone size was quantified from the wing pouch region,
709 by manually drawing boundaries using ImageJ. The ratio of total clone area to total area
710 of twin spot was computed and compared across different treatment or genotypes.

711

712 **4. Immunohistochemistry:**

713 Imaginal discs were fixed using 4% formaldehyde in 1× PBS, followed by 2 h
714 blocking with 0.5% bovine serum albumin (BSA) dissolved in 0.1% PBST (1×PBS with
715 0.1% Triton X-100). Primary antibody incubations were performed at 4°C overnight,
716 followed by 2 h secondary incubation at room temperature. All washes following
717 antibody incubation were performed in 0.1% PBST. Primary antibodies were against,
718 rabbit anti-cleaved Dcp-1 (Cell Signaling 9578, 1:200), mouse anti-γH2Av (DSHB UNC93-
719 5.2.1, 1:50), mouse anti-βGalactosidase (DSHB 40a-1, 1:50), mouse anti-p53 (DSHB 25F4,
720 1:50) and mouse anti-GFP (DSHB 12A6, 1:50), anti-Xrp1 (1:250; gift from Rio lab). Alexa-
721 Fluor (Thermo Fisher-Invitrogen) and Cyanine dye (Jackson labs) conjugated secondary
722 antibodies were used at 1:200 dilution. Image acquisition was performed on Leica-Sp8
723 microscope, and intensity adjustments were made using Photoshop CC 2018 and Image
724 J was used for image processing.

725 Previous experiments have supported that significant results could be obtained
726 from 5 replicates, in most of the cases more than 5 sample were analyzed. Experiments
727 were repeated at least 2 times or more for most of the results. No exclusion of the data
728 points was made while performing statistical significance. For the quantitative data N
729 values are indicted in the figure legends. Statistical significance was performed using
730 student t-test for independent or dependent means as indicated in figure legends. For
731 certain data sets one-way ANOVA with Bonferroni-Holm multiple comparison
732 correction was performed as mentioned in the figure legends. Exact p values are
733 indicated in the figures.

734

735 **5. q-RT PCR:**

736 Total RNA was extracted from wing imaginal discs of late third instar larvae
737 treated with 2000 Rads of IR, untreated larvae were taken as control for normalization.
738 Wing discs were collected in TRIzol reagents (Ambion) and RNA was isolated according
739 to the manufacturer's instructions. RNA samples were DNase treated according to
740 manufacturer's instructions (Thermo Fisher; AM1907) and reverse transcribed using
741 Verso cDNA Synthesis Kit (Thermo Fisher; AB1453). The cDNA was used to perform the
742 q-RT PCR reactions following the manufacturer's instructions for the TaqMan™ Fast
743 Advanced Master Mix (Thermo Fisher; 4444557). Custom design FAM-MGB TaqMan
744 probes were utilized for q-RT PCR. The gene expression values were normalized to
745 housekeeping gene RpL32 and were also confirmed with actin as a second control (data
746 not included). Following calculations were used for estimating fold change in gene
747 expression ΔCt = Ct (gene of interest) – Ct (housekeeping gene), ΔΔCt = ΔCt (3-4 hr IR) –
748 ΔCt (untreated average) and Fold gene expression = 2^ -(ΔΔCt). 3 biological replicates
749 were analysed for each condition and genotype. The gene expression analysis was
750 performed using technical triplicates for each sample. It has been previously established
751 that significant results can obtained 3 biological and 3 technical triplicates.
752 The following TaqMan probes were used in this study:

753 1. p53 Dm02154335_g1
754 2. Xrp1 Dm02142088_g1
755 3. rpr Dm01823054_s1
756 4. hid Dm01823031_m1
757 5. GstD1 Dm02362792_s1
758 6. eiger Dm01794373_m1
759 7. rad50 Dm01817359_g1
760 8. PolZ1 Dm01843262_g1
761 9. DNAlig4 Dm01838632_g1
762 10. Ku80 Dm01791676_g1
763 11. *Drosophila* RpL32 Dm02151827_g1
764 12. *Drosophila* actin Dm02361909_s1

765
766

767 FIGURES AND FIGURE LEGENDS:

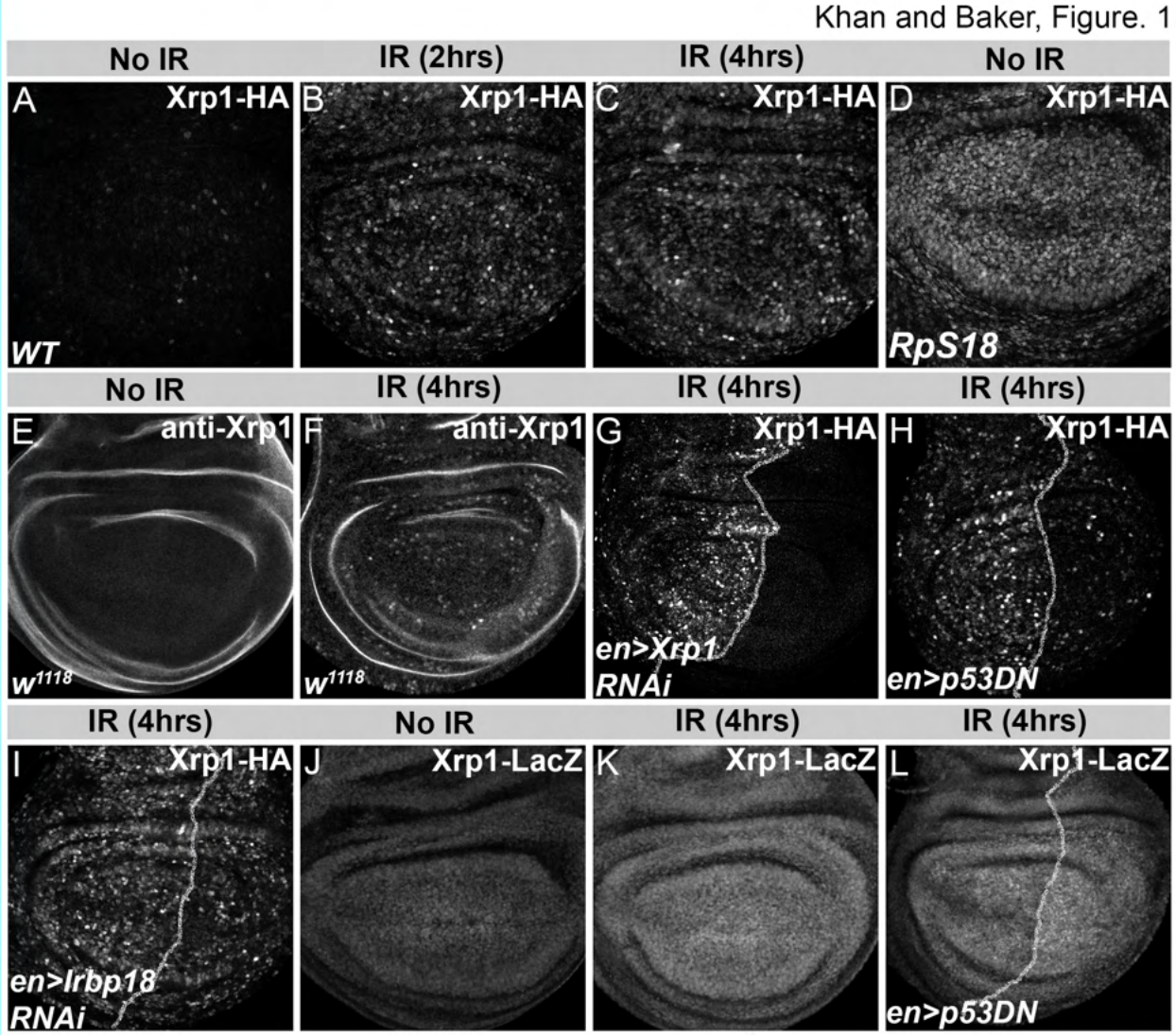

768
769
770 **Figure 1: DNA damage induced Xrp1 expression**

771 Xrp1 protein levels in the wild type III instar wing discs stained for HA, in 0 Rads
772 (control) (A), 2 hours after 1500 Rads (B), 4 hours after 1500 Rads (C) and in *Rp18*$^{+/-}$ mutant
773 (D). Larval wing discs stained with Xrp1 antibody, 0 Rads (control) (E) and 4 hours after
774 1500 Rads (F) (note: Xrp1 antibody show high noise to signal ratio compared to Xrp1-
775 HA). Xrp1-HA expression at 4 hours post 1500 Rads in the posterior compartment
776 compared relative to the anterior compartment taken as an internal control, *en-Gal4*
777 driving *UAS-Xrp1* RNAi (G), p53 dominant negative (*UAS-p53*^{H159N}) (H), and *UAS-Irbp18*
778 RNAi (I). III instar wing discs assayed for *Xrp1*^{02515}-lacZ enhancer trap expression detected
779 by anti-βgal antibody in 0 Rads (J), 4 hours after 1500 Rads (K) and in the wing disc

780 expressing *UAS-p53*^{H159N} under control of *en-Gal4*, 4 hours after 1500 Rads (L). N= 7-8 discs
781 were analyzed for every genotype, each experiment was repeated at least 2-3 times.
782 Genotypes: (A-C) *Xrp1-HA*, (D) *p{hs:FLP}; FRT42 RpS18 p{ubi:GFP}*, (E-F) *w*^{1118} (G) *en-*
783 *Gal4::UAS-RFP, UAS-Xrp1 RNAi* (VDRC 107860)*; Xrp1-HA*, (H) *en-Gal4::UAS-RFP, UAS-*
784 *p53DN*^{H159N} (Bl. 8420)*; Xrp1-HA*, (I) *en-Gal4::UAS-RFP, UAS-Irbp18 RNAi; Xrp1-HA*, (J-K)
785 *P{PZ}Xrp1*^{02515}, (L) *en-Gal4::UAS-RFP,UAS-p53DN*^{H159N} (Bl. 8420); *P{PZ}Xrp1*^{02515}
786

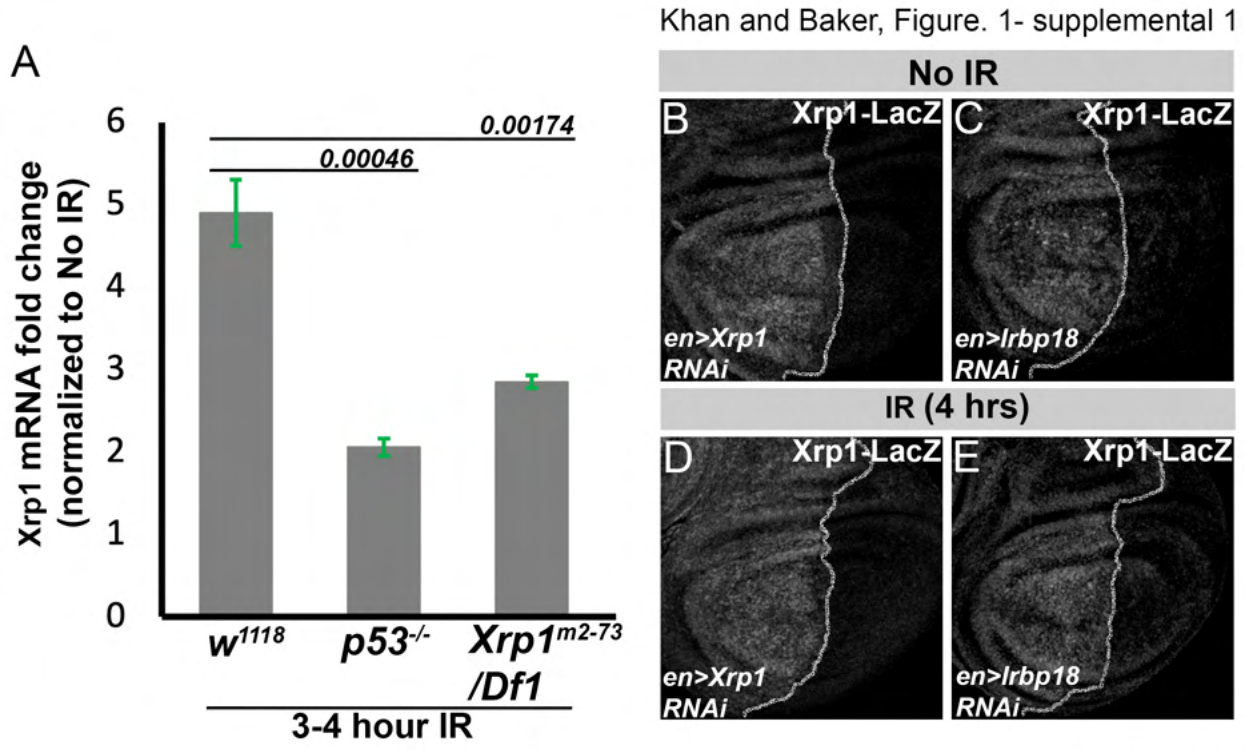

787
788 **Figure 1- Supplemental 1: Xrp1 RNA expression in response to DNA damage**
789 qRT-PCR analysis for Xrp1 mRNA expression levels from III instar wing discs from the
790 genotypes *w*^{1118}, *p53*$^{[5A-1-4]}$ and *Xrp1*$^{m2-73}$*/Df1* collected 3-4 hours after irradiation (1500
791 RADs) and normalized to untreated (0 Rads) sample (A). III instar wing discs assayed for
792 *Xrp1*^{02515}-lacZ enhancer trap expression by anti-βgal antibody in 0 Rads for *en>Xrp1 RNAi*
793 (B), *en>Irbp18 RNAi* (C) and 4 hours after 1500 Rads treatment in genotypes *en>Xrp1*
794 *RNAi* (D), *en>Irbp18 RNAi* (E). Number of wing discs analyzed for genotypes were N= 3
795 for B, N=2 for C, N=3 for D and N=5 for E, Data is plotted as mean± SEM, two-tailed
796 student t-test for independent means was performed for statistical significance.

797 Genotype: (A) *w*^{1118}, *yw; p53*$^{[5A-1-4]}$, and *Xrp1*$^{m2-73}$/ *Df 1*, (B & C) *en-Gal4::UAS-RFP, UAS-Xrp1*
798 *RNAi* (VDRC 107860); *P{PZ}Xrp1*^{02515} (C & E) *en-Gal4::UAS-RFP, UAS-Irbp18 RNAi;*
799 *P{PZ}Xrp1*^{02515}

Khan and Baker, Figure. 2

A

B

Gene category	Radiation induced p53- dependent genes (RIPD)	Common upregulated target genes between p53- RIPD and Xrp1 dependent genes from *Rp*$^{+/-}$ mutant RNA-seq data
Transcription factors	***Xrp1, Irbp18/CG6272***, *escl*	***Xrp1, Irbp18/CG6272***
Pro-apoptotic genes	***rpr, hid***, *skl, Corp, eiger, RnrL*	***rpr, hid***
DNA repair genes	***Irbp, Ku80, rad50, mre11, mus201, mus205, lig3, lig4, RpA-70, agt,, CG6171, CG5664,*** *CG13204*	***Irbp, Ku80, rad50, mre11, mus201, mus205, lig3, lig4, RpA-70, agt, CG6171, CG5664***
Redox genes	***CG9836/ISCU, CG11897***, *GstD5, spo, CG1718, pyd*	***CG9836/ISCU, CG11897***
Others	***Cul-2***, *Pka-C3*, ***eIF6, CG18596,*** *halo, cyp301a1, CG12194, CG15479, CG15658, CG10965, CG16815, CG5202, CG15480, CG13714*	***Cul-2, eIF6, CG18596***

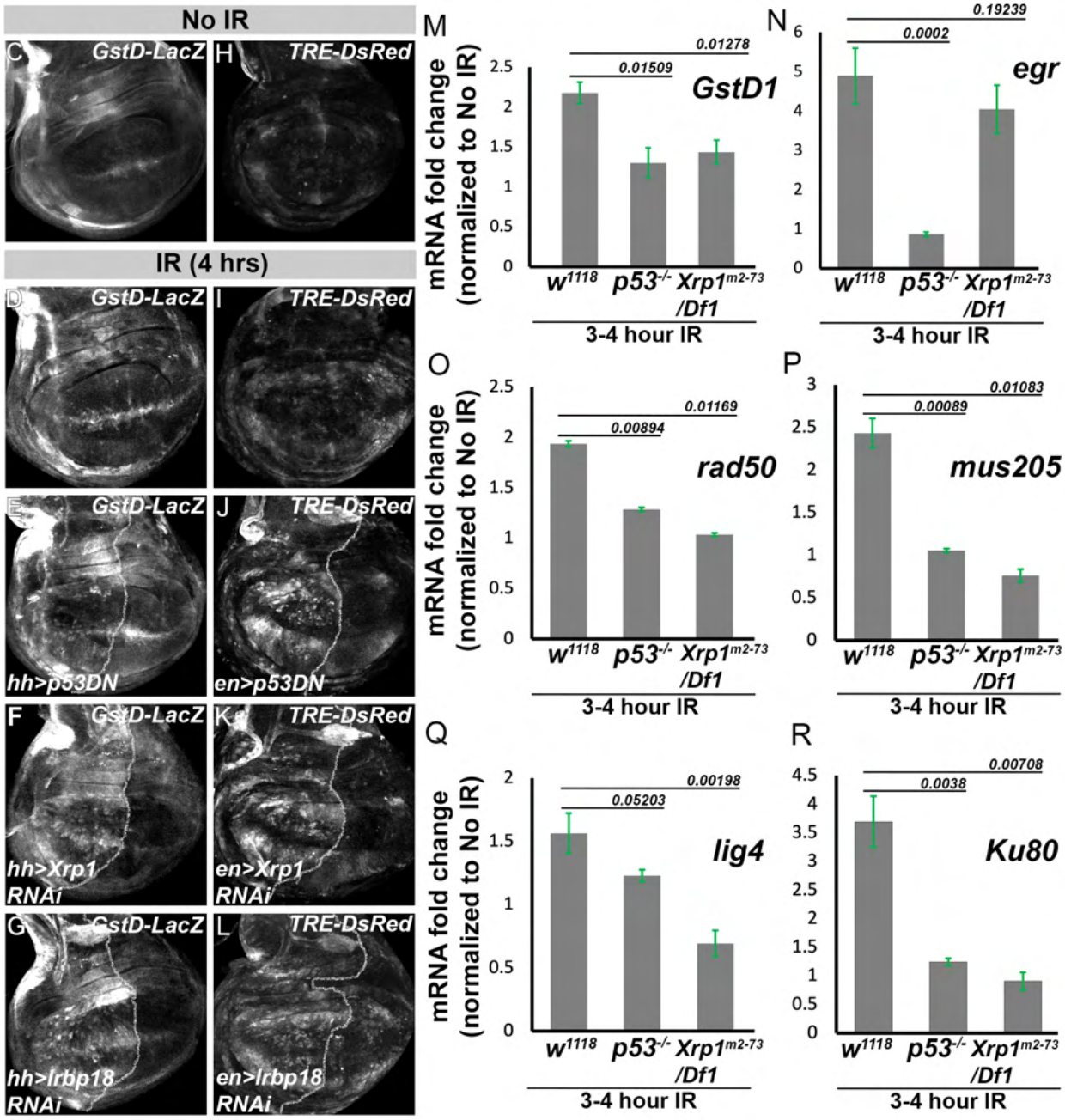

800

801 **Figure 2: Xrp1 serves as the effector of p53 in DNA damage response**
802 Vein diagram showing the overlap of p53 (Akdemir et al. 2007; Brodsky et al. 2004) and
803 Xrp1 (Lee et al. 2018; Baillon et al. 2018) target genes (A). Table showing the genes
804 organized according to GO categories from radiation-induced p53-dependent (RIPD) and
805 genes common between Xrp1- and p53- dependent transcription program (highlighted
806 in bold) (B). Expression of *GstD*-lacZ in III instar wing discs measured by staining for
807 anti-βgal antibody, in the wild type (no IR) (C), 4 hours after 2000 Rads in wild type disc
808 (D), *UAS-p53*^{H159N} (E), *UAS-Xrp1 RNAi* (F) and *UAS-Irbp18* RNAi (G). Expression of *TRE-*
809 *dsRed* in III instar wing discs measured by staining for anti-RFP antibody, in the wild type
810 (no IR) (H), 4 hours after 1500 Rads in wild type disc (I), *UAS-p53*^{H159N} (J). *UAS-Xrp1 RNAi*
811 (K) and *UAS-Irbp18 RNAi* (L). qRT-PCR analysis for mRNA expression levels from III
812 instar wing discs of *w*^{1118}, *p53*$^{[5A-1-4]}$ and *Xrp1*$^{m2-73}$*/Df1* collected 3-4 hours after irradiation
813 (1500 RADs) and normalized to untreated (0 Rads) sample, for the following genes *GstD1*
814 (M), *egr* (N), *rad50* (O), *mus205* (P), *lig4* (Q) and *Ku80* (R). N= 7-8 discs were analyzed for
815 every genotype, each experiment was repeated at least 2-3 times. Data is plotted as
816 mean± SEM, two-tailed student t-test for independent means was performed for
817 statistical significance.
818 Genotype: (C & D) *GstD-LacZ,* (E) *GstD-LacZ, UAS-p53*^{H159N} (Bl. 8420)*; hh-Gal4::UAS-GFP,*
819 (F) *GstD-LacZ, UAS-Xrp1 RNAi* (VDRC 107860)*; hh-Gal4::UAS-GFP,* (G) *GstD-LacZ, UAS-*
820 *Irbp18 RNAi; hh-Gal4::UAS-GFP*, (H and I) *TRE-dsRed,* (J) *TRE-dsRed::en-Gal4, UAS-*
821 *p53*^{H159N} (Bl. 8420), (K) *TRE-dsRed::en-Gal4, UAS-Xrp1 RNAi* (VDRC 107860), (L) *TRE-*
822 *dsRed::en-Gal4, UAS-Irbp18 RNAi*, (M-R) *w*^{1118}, *yw; p53*$^{[5A-1-4]}$, and *Xrp1*$^{m2-73}$*/Df1*
823

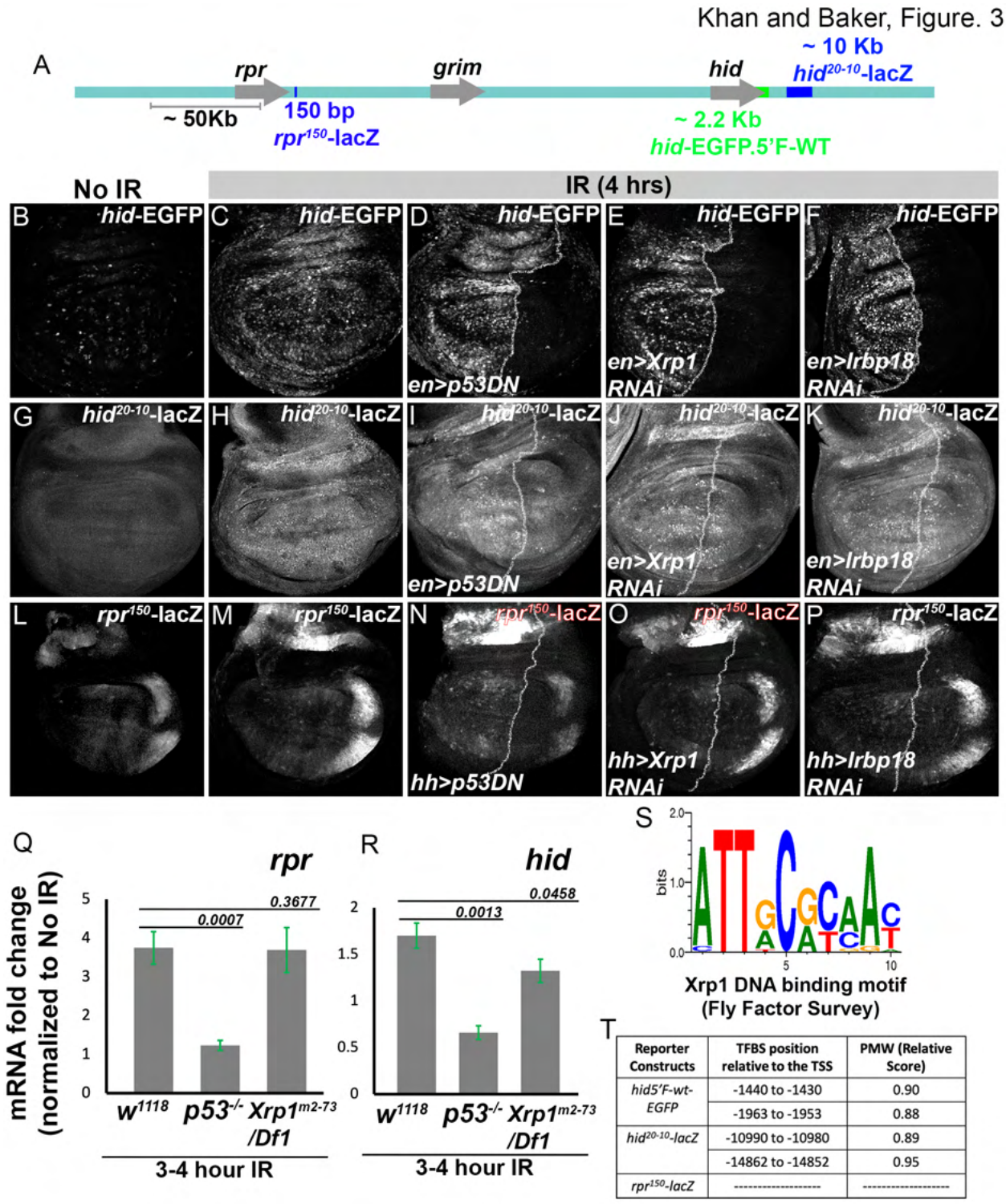

Reporter Constructs	TFBS position relative to the TSS	PMW (Relative Score)
hid5'F-wt-EGFP	-1440 to -1430	0.90
	-1963 to -1953	0.88
hid20-10-lacZ	-10990 to -10980	0.89
	-14862 to -14852	0.95
rpr150-lacZ	----------	----------

Figure 3: Xrp1 controls expression of the regulatory sequences of pro-apoptotic gene *hid*

Schematic of H99 locus with approximate positions of the *rpr, hid,* and *grm* and the reporter lines used for the analysis (A). Expression of *hid5'F-wt-EGFP* measured by

829 staining for anti-GFP antibody, in the wild type (no IR) (B) and 4 hours after 2000 Rads
830 in wild type wing disc (C), *UAS-p53*^{H159N} (D), *UAS-Xrp1 RNAi* (E) and *UAS-Irbp18* RNAi
831 (F). *hid*$^{20\text{-}10}$*-lacZ* expression measured by anti-βgal staining, in the wild type (no IR) (G)
832 and 4 hours after 2000 Rads in wild type wing disc (H), *UAS-p53*^{H159N} (I), *UAS-Xrp1* (J)
833 and *UAS-Irbp18* RNAi (K). *rpr*^{150}*-lacZ* expression measured by anti-βgal staining, in the
834 wild type (no IR) (L) and 4 hours after 2000 Rads in wild type wing disc (M). *UAS-p53*^{H159N}
835 (N), *UAS-Xrp1* (O) and *UAS-Irbp18* RNAi (P). qRT-PCR analysis for mRNA expression
836 levels from III instar wing discs of *w*^{1118}, *p53*$^{[5A\text{-}1\text{-}4]}$ and *Xrp1*$^{m2\text{-}73}$*/Df1* collected 3-4 hours after
837 irradiation (1500 RADs) and normalized to untreated (0 Rads) sample, for the following
838 genes, *rpr* (Q), and *hid* (R). Putative DNA binding motif of Xrp1/Irbp18 heterodimer,
839 adapted from Fly Factor Survey (S). Position of Xrp1/Irbp18 DNA motif in the upstream
840 regulatory region of *hid* relative to the TSS (T). N= 5-8 discs was analyzed for every
841 genotype, each experiment was repeated at least 2-3 times. Data is plotted as mean± SEM,
842 two-tailed student t-test for independent means was performed for statistical
843 significance.
844 Genotype: (B & C) *hid5'F-wt-EGFP*, (D) *hid5'F-wt-EGFP; en-Gal4::UAS-RFP, UAS-p53*^{H159N}
845 (Bl. 8420), (E) *hid5'F-wt-EGFP; en-Gal4::UAS-RFP, UAS-Xrp1 RNAi* (VDRC 107860), (F)
846 *hid5'F-wt-EGFP; en-Gal4::UAS-RFP, UAS-Irbp18 RNAi*, (G & H) *yw*; *hid*$^{20\text{-}10}$*-lacZ*, (I) *en-*
847 *Gal4::UAS-RFP, UAS-p53*^{H159N} (Bl. 8420)*; hid*$^{20\text{-}10}$*-lacZ*, (J) *en-Gal4::UAS-RFP, UAS-Xrp1*
848 *RNAi* (VDRC 107860)*; hid*$^{20\text{-}10}$*-lacZ*, (K) *en-Gal4::UAS-RFP, UAS-Irbp18 RNAi; hid*$^{20\text{-}10}$*-lacZ*,
849 (L & M) *rpr*^{150}-lacZ, (N) *rpr*^{150}*-lacZ, UAS-p53*^{H159N} (Bl. 8420)*; hh-Gal4::UAS-GFP*, (O) *rpr*^{150}*-*
850 *lacZ, UAS-Xrp1 RNAi* (VDRC 107860)*; hh-Gal4::UAS-GFP,* (P) *rpr*^{150}*-lacZ, UAS-Irbp18*
851 *RNAi; hh-Gal4::UAS-GFP*, (Q-R) *w*^{1118}, *yw; p53*$^{[5A\text{-}1\text{-}4]}$, and *Xrp1*$^{m2\text{-}73}$*/Df1*
852

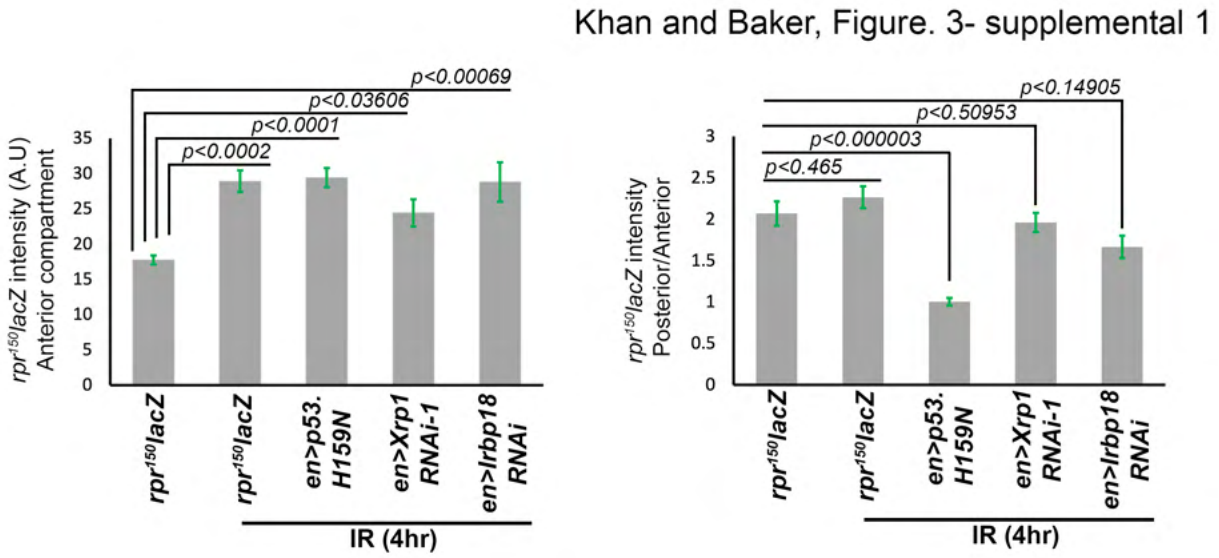

Figure 3- Supplemental 1: *rpr^{150}lacZ* intensity quantification

Average intensity quantification for *rpr^{150}lacZ* from the wing the anterior compartment of the wing pouch with and without IR, for the genotypes shown in Figure 3 L-P. *rpr^{150}lacZ* average intensity in the anterior compartments is elevated by IR, regardless of gene expression or depletion in the P compartments (A). The ratio of mean posterior to mean anterior LacZ expression for each. Only p53-DN reduced the relative *rpr-LacZ* expression level (B). Statistics: Data is plotted as mean± SEM; n=5 for *irbp18* RNAi, n=7 for other genotypes; significance assessed by one-way Anova with Bonferroni-Holm multiple comparison correction. For panel B, genotypes were compared only to the unirradiated control.

Figure 3 - source data file 1: intensity quantification for *rpr^{150}lacZ*

Genotype: (A & B) *rpr^{150}*-lacZ**,** *rpr^{150}-lacZ, UAS-p53^{H159N}* (Bl. 8420)*; hh-Gal4::UAS-GFP***,** *rpr^{150}-lacZ, UAS-Xrp1 RNAi* (VDRC 107860)*; hh-Gal4::UAS-GFP, rpr^{150}-lacZ, UAS-Irbp18 RNAi; hh-Gal4::UAS-GFP*

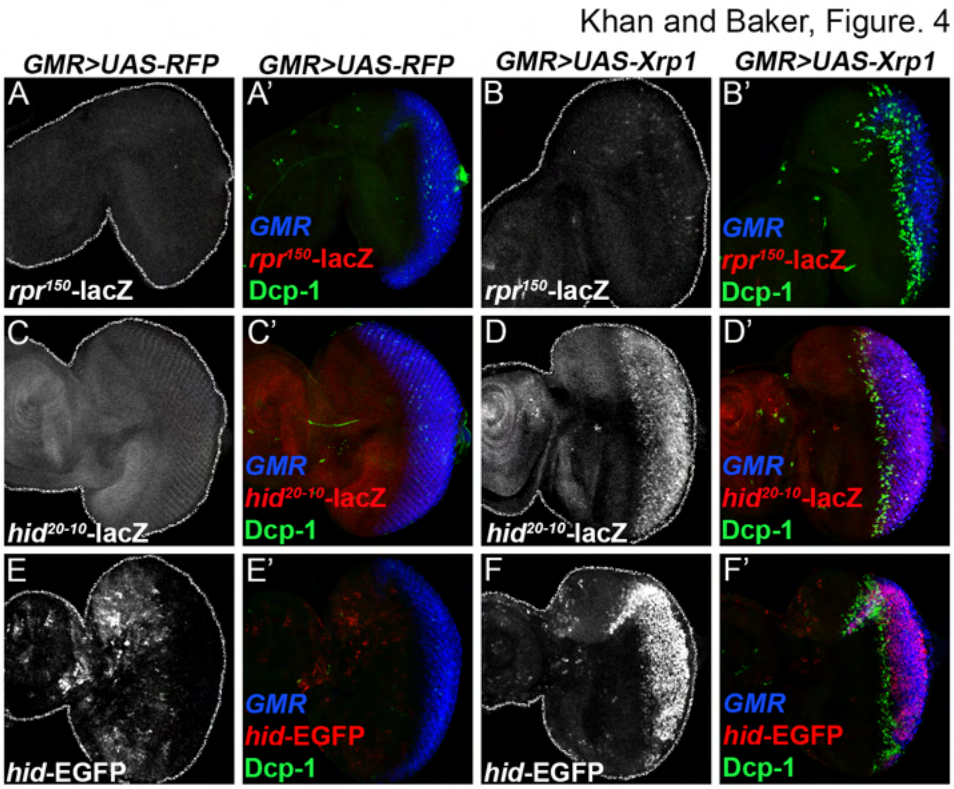

Figure 4: Xrp1 is sufficient for the expression of p53- dependent DDR target genes

rpr^{150}*-lacZ* reporter expression measured by anti-βgal (red) and cell death by anti-Dcp-1 (green) in III instar eye imaginal disc expressing UAS-RFP (A) and UAS-Xrp1 long isoform (B), under the control of *GMR-Gal4* (blue). *hid*$^{20\text{-}10}$*-lacZ* reporter expression measured by anti-βgal (red) and cell death by anti-Dcp-1 (green) in III instar eye imaginal disc expressing UAS-RFP (C) and UAS-Xrp1 long isoform (D) under the control of *GMR-Gal4* (blue). *hid5′F-wt-EGFP* reporter expression measured by anti-GFP (red) and cell death by anti-Dcp-1 (green) in III instar eye imaginal disc expressing UAS-RFP (E) and UAS-Xrp1 long isoform (F) under the control of *GMR-Gal4* (blue). N= 7-8 discs were analyzed for every genotype; each experiment was repeated at least 2 times. All the control and experimental genotypes shown in this figure were kept at 18^{0}C in order to lessen the effect of Xrp1 overexpression.

Genotype: (A-A′) *GMR-Gal4::UAS-RFP, rpr*^{150}*-lacZ*, (B-B′) *GMR-Gal4::UAS-RFP::UAS-Xrp1, rpr*^{150}*-lacZ*, (C-C′) *GMR-Gal4::UAS-RFP; hid*$^{20\text{-}10}$*-lacZ*, (D-D′) *GMR-Gal4::UAS-RFP::UAS-Xrp1; hid*$^{20\text{-}10}$*-lacZ*, (E-E′) *hid5′F-wt-EGFP; GMR-Gal4::UAS-RFP*, (F-F′) *hid5′F-wt-EGFP; GMR-Gal4::UAS-RFP, UAS-Xrp1*

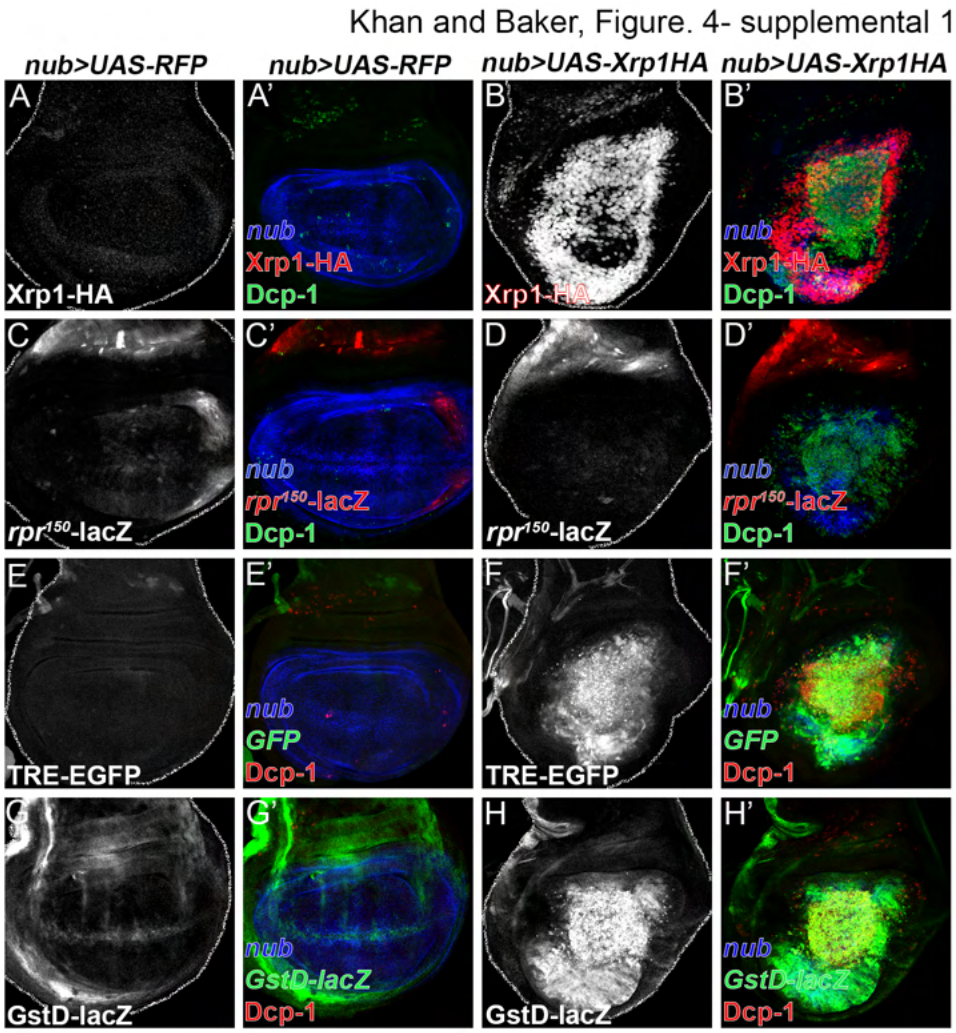

Figure 4- Supplemental 1: Xrp1 is sufficient for the expression of p53- dependent DDR target genes

Xrp1-HA protein measured by anti-HA (red) and cell death by Dcp-1 (green) in the III instar wing disc expressing UAS-RFP control (A) and UAS-Xrp1 long isoform (B) under the control of *nub-Gal4* (blue). *rpr*^{150}*-lacZ* reporter expression measured by anti-βgal (red) and cell death by anti-Dcp-1 (green) in III instar wing imaginal disc expressing UAS-RFP (C) and UAS-Xrp1 (D) under the control of *nub-Gal4*. *TRE-EGFP* reporter expression measured by anti-GFP (red) and cell death by anti-Dcp-1 (green) in III instar wing imaginal disc expressing UAS-RFP control (E) and UAS-Xrp1 (F) under the control of *nub-Gal4* (blue). *GstD-lacZ* reporter expression measured by anti-GFP (red) and cell death by anti-Dcp-1 (green) in III instar wing imaginal disc expressing UAS-RFP (G) and UAS-Xrp1 (H) under the control of *nub-Gal4* (blue). N= 7-8 discs were analyzed for every genotype, each experiment was repeated at least 2 times. All the control and experimental

901 genotypes shown in this figure were kept at 18^{0}C in order to lessen the effect of Xrp1
902 overexpression.
903 Genotype: (A) *nub-Gal4::UAS-RFP*, (B) *nub-Gal4::UAS-RFP::UAS-Xrp1-HA*, (C) *nub-*
904 *Gal4::UAS-RFP*, *rpr^{150}-lacZ*, (D) *nub-Gal4::UAS-RFP::UAS-Xrp1-HA*, *rpr^{150}-lacZ*, (E) *nub-*
905 *Gal4::UAS-RFP*, *TRE-GFP*, (F) *nub-Gal4::UAS-RFP::UAS-Xrp1-HA*, *TRE-GFP*, (G) *nub-*
906 *Gal4::UAS-RFP*, *GstD-lacZ*, (H) *nub-Gal4::UAS-RFP::UAS-Xrp1-HA*, *GstD-lacZ*
907

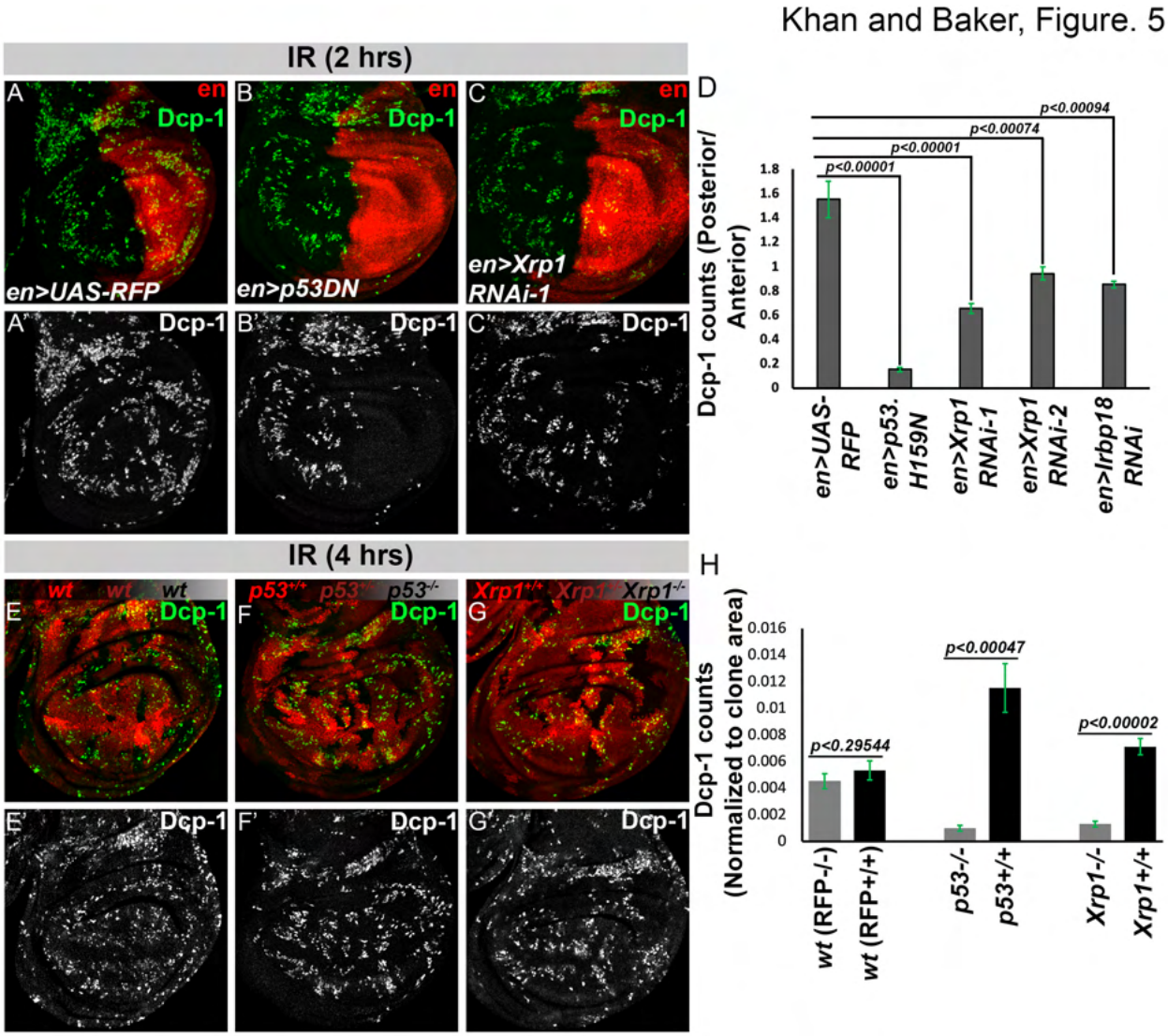

908
909 **Figure 5: Xrp1 is partly required for DNA damage induced cell death**
910 *Drosophila* III instar wing imaginal discs dissected at 2 hours after 1500 Rads, cell death is
911 measured by Dcp-1 (green and gray scale) in different genetic perturbations using en-
912 Gal4 (posterior compartment (red)), UAS-RFP (A), *UAS-p53^{H159N}* (B) and *UAS-Xrp1* RNAi

913 (C). Dcp-1 positive cells were quantified and plotted as the ratio of the number of Dcp-1
914 positive cells in anterior and posterior compartment (D). Wing discs dissected 4 hours
915 after 1500 RADs and stained for Dcp-1 positive cells in *FRT82* (E), *FRT82p53*$^{[5A-1-4]}$ (F), and
916 *FRT82Xrp1*$^{m2-73}$ (G). (H) Dcp-1 positive cells quantified inside the clone (RFP-/-) and
917 inside the sister clone (RFP+/+). 4 hours timepoint was taken to have uniform
918 distribution of Dcp-1 positive cells. Statistics: (A-D) N= 15 each genotype. (E-H) N= 8
919 each genotype. Data is plotted as mean± SEM, two-tailed student t-test for independent
920 means for (A-D) and for dependent mean for (E-H) was performed for statistical
921 significance.
922 Figure 5 - source data file 1: intensity quantification for Dcp1 (Figure 5A-D)
923 Figure 5 - source data file 2: intensity quantification for Dcp1 (Figure 5E-H)
924
925 Genotype: (A) *en-Gal4::UAS-RFP,* (B) *en-Gal4::UAS-RFP, UAS-p53DN*^{H159N} (Bl. 8420), (C)
926 *en-Gal4::UAS-RFP, UAS-Xrp1 RNAi* (Bl. 34521), (E) *p{hs:FLP}; FRT82-RFP/FRT82* (30 min
927 hs, 48 hr A.E.L), (F) *p{hs:FLP}; FRT82-RFP/FRT82-p53*$^{[5A-1-4]}$ (30 min hs, 48 hr A.E.L), (G)
928 *p{hs:FLP}; FRT82-RFP/FRT82-Xrp1*$^{m2-73}$ (30 min hs, 48 hr A.E.L)
929

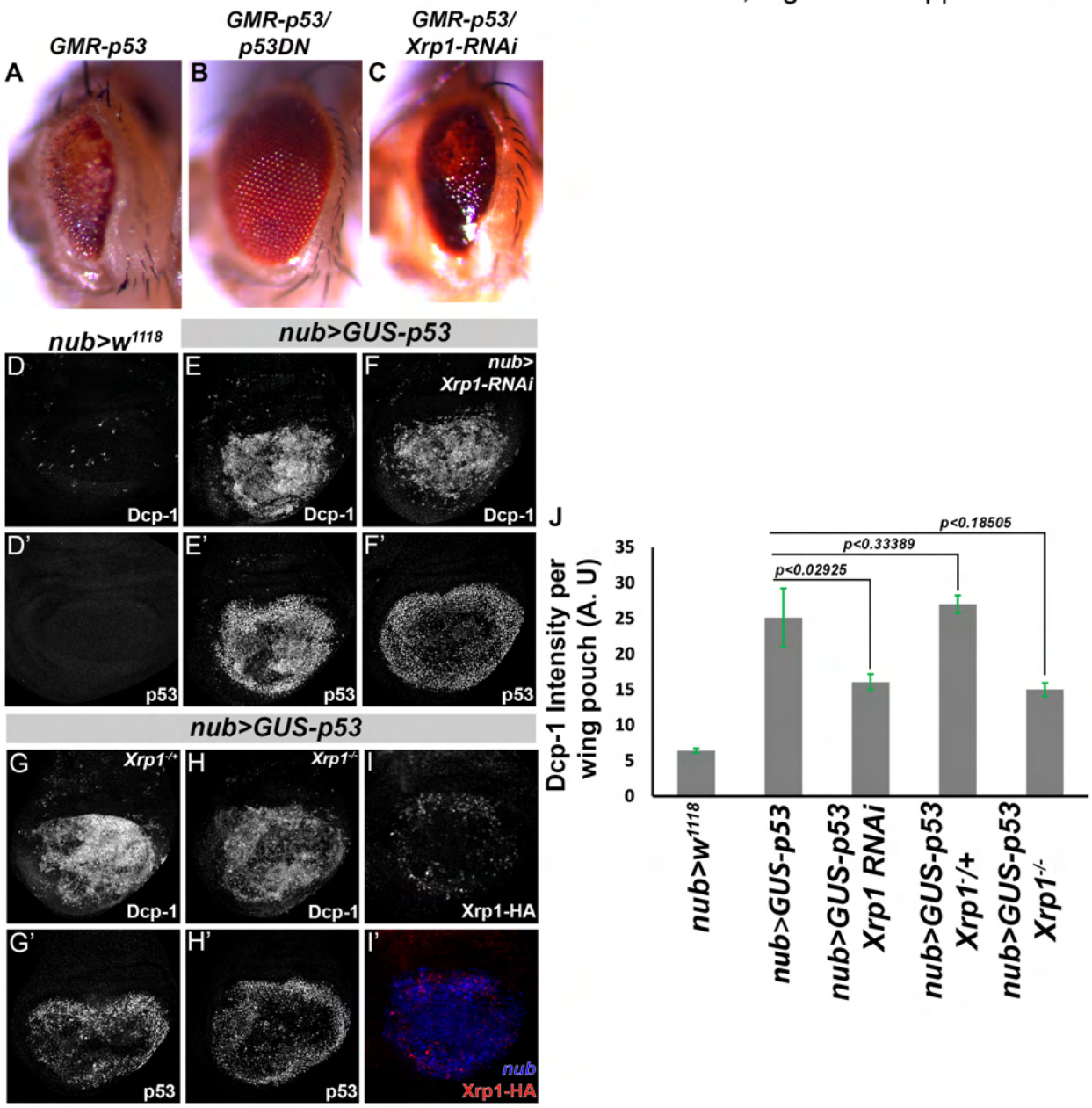

Figure 5- Supplemental 1: Xrp1 do not rescue p53 O/E phenotype

(A) Bright field photograph of *Drosophila* eye, rough eye phenotype due to constitutive expression of p53 under the control of GMR-promoter (*GMR-p53*). (B) Overexpression of dominant-negative p53 (*UAS-p53*^{H159N}) rescue the rough eye phenotype. (C) Xrp1 knock down by RNAi have slight effect on rough eye phenotype. (D) Control *nub-Gal4* exhibit few Dcp-1 positive cells and no p53 protein was detected by anti-p53 antibody. (E) *nub-Gal4* driving p53 overexpression (*GUS-p53*) in the wing pouch exhibit elevated cell death measured by Dcp-1 as well as p53 protein measured by anti-p53 antibody. (F) Co-

939 expressing *UAS-Xrp1* RNAi and *GUS-p53* under *nub-Gal4* lead to a decrease in cell death
940 by approximately 50%. (G) Removing one copy by $Xrp1^{m2-73}$/+ had no effect on cell death.
941 (H) Removing both copies of Xrp1 ($Xrp1^{m2-73}$/$Xrp1^{attp\ flox}$) lead to a decrease in cell death by
942 approximately 50%. Xrp1-HA expression assayed by anti-HA antibody in wing disc
943 expressing p53 under control of *nub-Gal4* (I & I′). (J) Dcp1 intensity was quantified using
944 ImageJ, N=6 for each genotype. Data is plotted as mean± SEM, two-tailed student t-test
945 for independent means. All the control and experimental genotypes shown in this figure
946 were kept at 18^0C to lessen the effect of p53 overexpression.
947 Figure 5 supplemental 1- source data file 1: Dcp1 quantification D-H and J
948
949 Genotype: (A) *GMR-p53,* (B) *GUS-p53, GMR-Gal4; UAS-p53*^{H159N} (Bl. 4021), (C) *GUS-p53,*
950 *GMR-Gal4; UAS-Xrp1 RNAi* (Bl. 4521), (D) *nub-Gal4;* w^{1118}, (E) *nub-Gal4, GUS-p53*, (F) *nub-*
951 *Gal4, GUS-p53; UAS-Xrp1 RNAi* (Bl. 4521), (G) *nub-Gal4, GUS-p53;* $Xrp1^{m2-73}$/+, (H) *nub-*
952 *Gal4, GUS-p53;* $Xrp1^{m2-73}$/$Xrp1^{attp\ flox}$, (I) *nub-Gal4, GUS-p53; Xrp1-HA*
953

Khan and Baker, Figure. 6

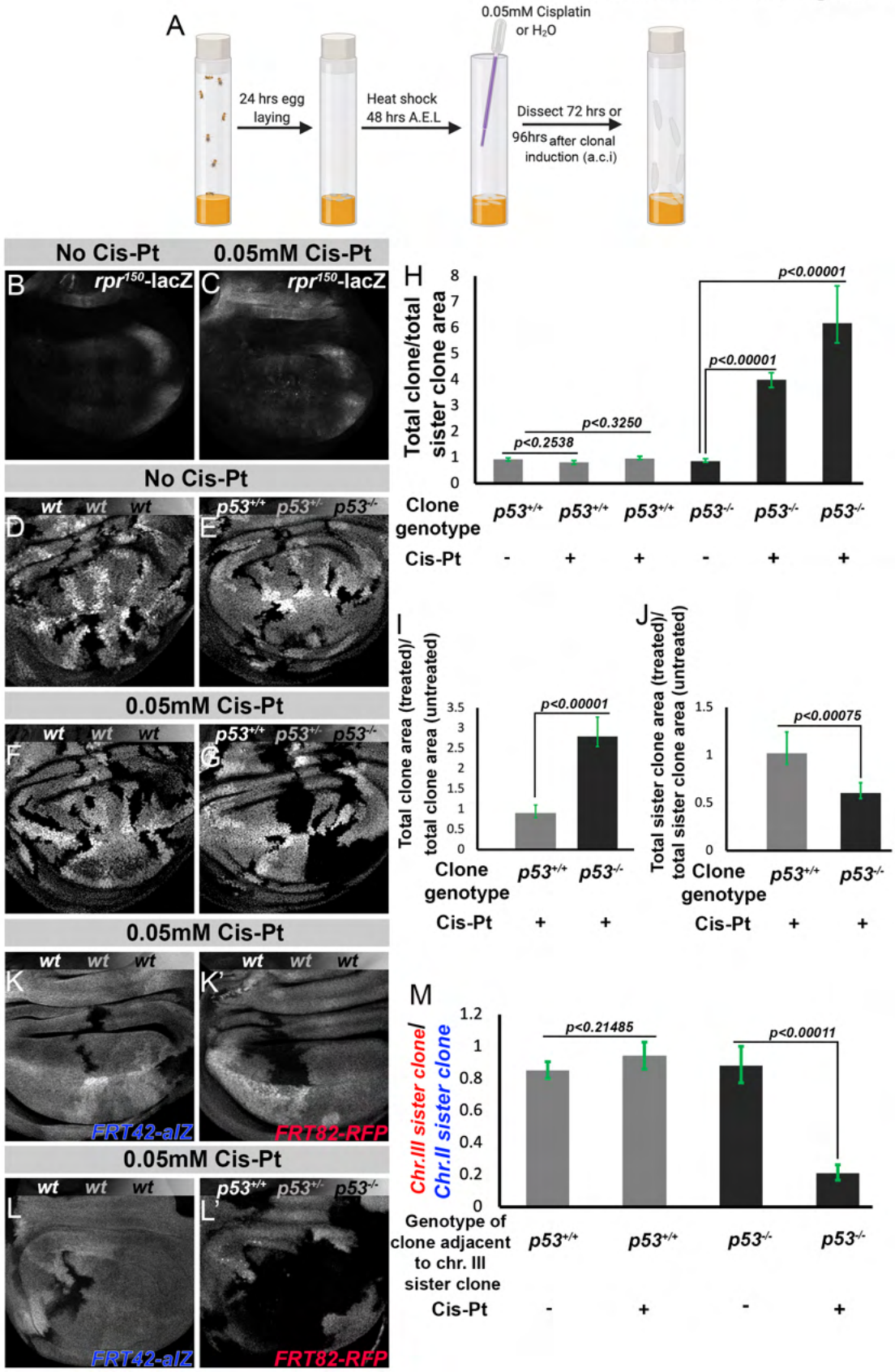

954

955 **Figure 6: Chronic exposure to sub-lethal genotoxic drug gives competitive advantage**
956 **to *p53* mutant over wild type cells**
957 (A) Schematic describing the timing for Cis-Pt treatment, clonal induction and dissection
958 time point (made using BioRender software). (B-C) *rpr*^{150}-*lacZ* reporter expression in III
959 instar wing imaginal disc measured by anti-βgal in control no Cis-Pt and 96 hours after
960 0.05mM Cis-Pt treatment. (D-G) III instar wing imaginal disc stained for RFP,
961 heterozygous cells one copy RFP (intermediate grey), sister clone with two copy of RFP
962 (dark grey) and clone marked by absence of RFP (black), 76 hours after clonal induction
963 (a.c.i) untreated discs (no Cis-Pt) *FRT82* (D) & *FRT82p53*$^{[5A-1-4]}$ (E) and 96 hours a.c.i +
964 0.05mM Cis-Pt treatment in *FRT82* (F) & *FRT82p53*$^{[5A-1-4]}$ (G). (H) Total clone (*FRT82/82*) to
965 sister clone (*FRT82-RFP/82-RFP*) area measurements in individual discs plotted as ratio
966 at 72 hours a.c.i in no Cis-Pt, 72 hours a.c.i + 0.05mM Cis-Pt and 96 hours a.c.i + 0.05mM
967 Cis-Pt. (I) Untreated (no Cis-Pt) clone to treated (0.05mM Cis-Pt) clone area ratio
968 (calculated per disc) for *FRT82* clone and for *p53*$^{-/-}$ mutant clone after 72 hours a.c.i. (J)
969 Ratio of *FRT82* sister clone (*FRT82-RFP/82-RFP*) to *p53*$^{+/+}$ sister clone (*FRT82-RFP/82-RFP*)
970 72 hours a.c.i in untreated discs (no Cis-Pt) and 0.05mM Cis-Pt. (K-L) Neutral clone assay
971 for confirming competitive disadvantage of sister clone associated with *p53*$^{-/-}$ mutant
972 clones, images are shown for 0.05mM Cis-Pt condition. Control disc (*FRT42-alz/FRT42;*
973 *Frt82-RFP*) with *FRT42* clone and its sister clone (*FRT42-alz/42-alz*) (K) and the same disc
974 with *FRT82* clone and its sister clone (*FRT82-RFP/82-RFP*) (K'). Experimental disc (*FRT42-*
975 *alz/FRT42; FRT82p53*$^{[5A-1-4]}$) carrying *FRT42* clone and its sister clone (*FRT42-alz/42-alz*) (L),
976 the same disc with *p53*$^{-/-}$ mutant clone and sister clone (*FRT82-RFP/82-RFP*) (L').
977 Measurements of *FRT42-alz/42-alz* sister clone to *FRT82-RFP/82-RFP* sister clone area
978 under no Cis-Pt 72 hours a.c.i and 0.05mM Cis-Pt at 96 hours a.c.i in control discs and the
979 *FRT42-alz/42-alz* sister clone to *FRT82-RFP/82-RFP* sister clone ratio in experimental discs
980 in no Cis-Pt at 72 hours a.c.i and 0.05mM Cis-Pt 96 hours a.c.i (M). Note: for neutral clone
981 assay the discs with non-overlapping *FRT42-alz* and *FRT82-RFP* were analyzed. This was
982 done to avoid any effect of lack of p53 mutant clone on *FRT42-alz* clone within the same
983 discs. Statistics: N= 10 discs each genotype (for D-J), data is plotted as mean± SEM, two-
984 tailed student t-test for independent means was performed for statistical significance. N
985 = 8 for (K-M), data is plotted as mean± SEM, two-tailed student t-test for dependent
986 means was performed for statistical significance.

987 Figure 6 - source data file 1: Clone and sister clone area quantification D-J
988 Figure 6 - source data file 2: Clone and sister clone area measurement for neutral clone
989 assay K-M
990
991 Genotype: (B & C) *rpr*^{150}-lacZ, (D) *p{hs:FLP}; FRT82-RFP/ FRT82* (30 min hs, 48 hr A.E.L),
992 (E) *p{hs:FLP}; FRT82-RFP/ FRT82-p53*$^{[5A-1-4]}$ (30 min hs, 48 hr A.E.L), (F) *p{hs:FLP}; FRT82-*
993 *RFP/ FRT82* (30 min hs, 48 hr A.E.L), (G) *p{hs:FLP}; FRT82-RFP/ FRT82-p53*$^{[5A-1-4]}$ (30 min
994 hs, 48 hr A.E.L), (K & K') *p{hs:FLP}; FRT42-alZ/ FRT42; FRT82-RFP/ FRT82* (20 min hs, 36
995 hr A.E.L), (L & L') *p{hs:FLP}; FRT42-alZ/ FRT42; FRT82-RFP/ FRT82-p53*$^{[5A-1-4]}$ (20 min hs,
996 36 hr A.E.L)
997

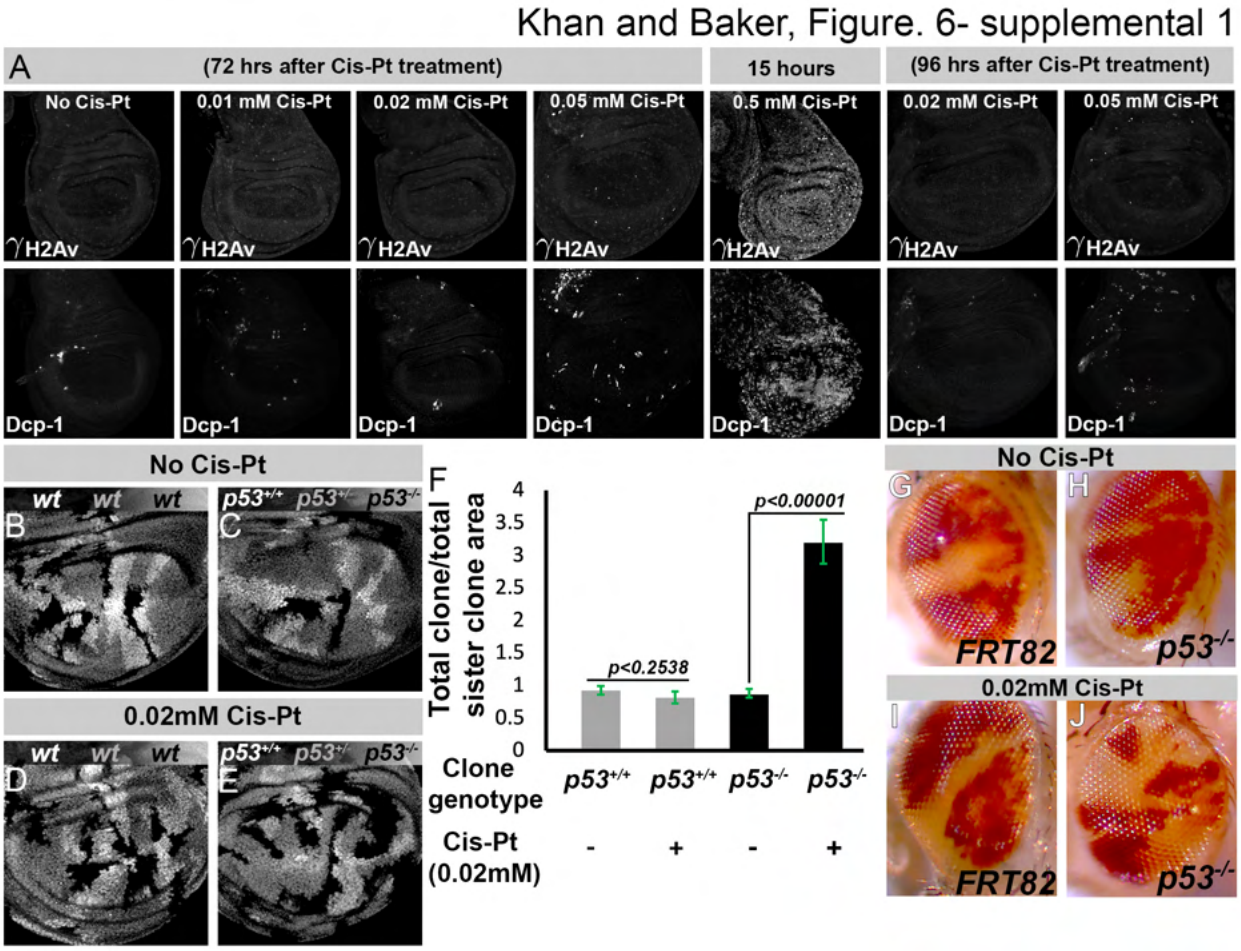

998
999 **Figure 6- Supplemental 1: Sub-cell lethal dosage of Cis-Pt do not cause heightened cell**
1000 **death but give competitive advantage to *p53*$^{-/-}$ mutant cells**

1001 (A) III instar wing imaginal discs assayed for cell death by anti-Dcp-1 staining and DNA
1002 damage by anti-γH2Av antibody at different concentrations (0.01mM, 0.02mM, 0.05mM
1003 and 0.5mM) of Cis-Pt at two different time points 72 or 96 hours after the treatment, as
1004 marked in the figure. 0.5mM Cisplatin samples were analyzed at 15 hours' time point due
1005 difficulty in recovering viable larvae at later time point 72 and 96 hours. (B-E) III instar
1006 wing imaginal disc stained for RFP, heterozygous cells one copy RFP (intermediate grey),
1007 sister clone with two copy of RFP (dark grey) and clone is marked by absence of RFP
1008 (black) 72 hours after clonal induction in *FRT82* (B), *FRT82p53*$^{[5A-1-4]}$ (C) and 72 hours after
1009 clonal induction (a.c.i) + 0.02mM Cis-Pt treatment in *FRT82* (D) & *FRT82p53*$^{[5A-1-4]}$ (E). (F)
1010 Total clone to sister clone (*FRT82-RFP/82-RFP*) area measurements in individual discs,
1011 plotted as ratio at 72 hours a.c.i in no Cis-Pt, and 72 hours a.c.i + 0.02mM Cis-Pt treatment.
1012 (G-J) Bright field photograph of adult eye in untreated larvae (no Cis-Pt treatment) in
1013 *FRT82* (G) & *FRT82p53*$^{[5A-1-4]}$ (H), and in treated larvae (0.02mM Cis-Pt treatment) *FRT82*
1014 (I) & *FRT82p53*$^{[5A-1-4]}$ (J). N= 10 discs each genotype in (B-F), data is plotted as mean± SEM,
1015 two-tailed student t-test for independent means was performed for statistical
1016 significance.
1017 Figure 6 – Supplemental 1- source data file 1: Clone size quantification B-F
1018
1019 Genotype: (A) *w*^{1118}, (B-D) *p{hs:FLP}; FRT82-RFP/FRT82* (30 min hs, 48 hr A.E.L), (C-E)
1020 *p{hs:FLP}; FRT82-RFP/FRT82-p53*$^{[5A-1-4]}$ (30 min hs, 48 hr A.E.L), (G-I) *eyflp; FRT82-*
1021 *RFP/FRT82,* (H-J) *eyflp; FRT82-RFP/FRT82-p53*$^{[5A-1-4]}$
1022

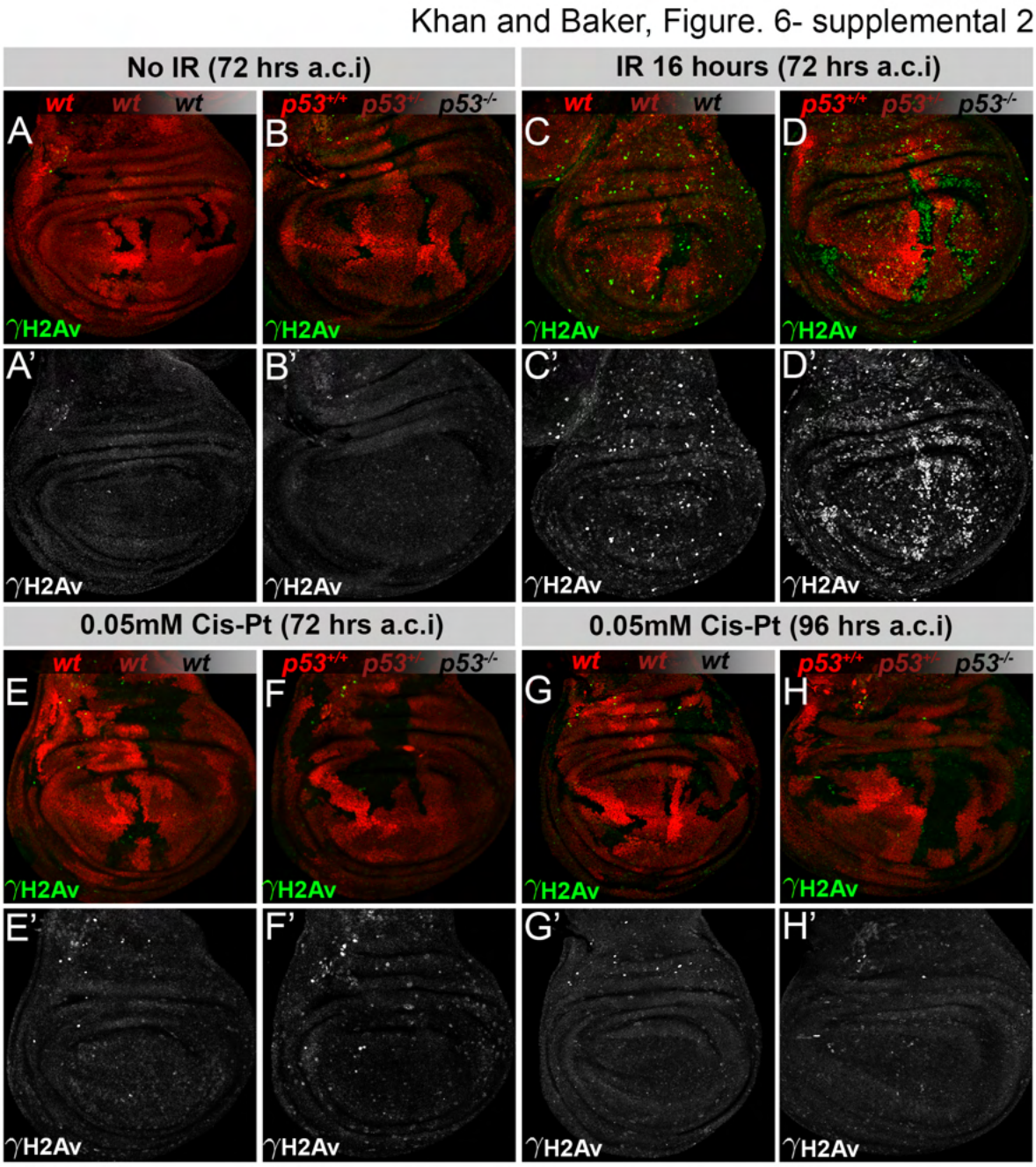

1023

1024 **Figure 6- Supplemental 2: *p53*$^{-/-}$ mutant and wild clone do not show any significant**
1025 **differences in DDR upon 0.05mM Cis-Pt**

1026 III instar wing imaginal discs stained for γH2Av (green and grey scale) and marked for
1027 clone (Black), sister clone (bright red) and heterozygous tissue (dull red). (A-B) γH2Av
1028 levels in *FRT82* (A), and *FRT82p53*$^{[5A-1-4]}$ (B) under no Cis-Pt condition after 72 hours after
1029 clonal induction (a.c.i). (C-D) 1500 Rads γ-radiation showed significantly higher levels of
1030 γH2Av, no significant difference was observed between clone and sister clone of *FRT82*

(C), *p53*$^{-/-}$ mutant clone showing higher number of γH2Av positive cells compared to sister clone (D). (E-H) Slight overall increase in γ-H2Av level upon 0.05mM Cisplatin treatment in *FRT82* (E), and *FRT82p53*$^{[5A-1-4]}$ (F) at 72 hours a.c.i and *FRT82* (G), and *FRT82p53*$^{[5A-1-4]}$ (H) at 96 hours a.c.i. N = 15 discs observed and compared for γ-H2Av staining for each genotype, experiment was repeated at least 2-3 times.

Genotype: (A, C, E & G) *p{hs:FLP}; FRT82-RFP/FRT82* (30 min hs, 48 hr A.E.L), (B, D, F & H) *p{hs:FLP}; FRT82-RFP/ FRT82-p53*$^{[5A-1-4]}$ (30 min hs, 48 hr A.E.L)

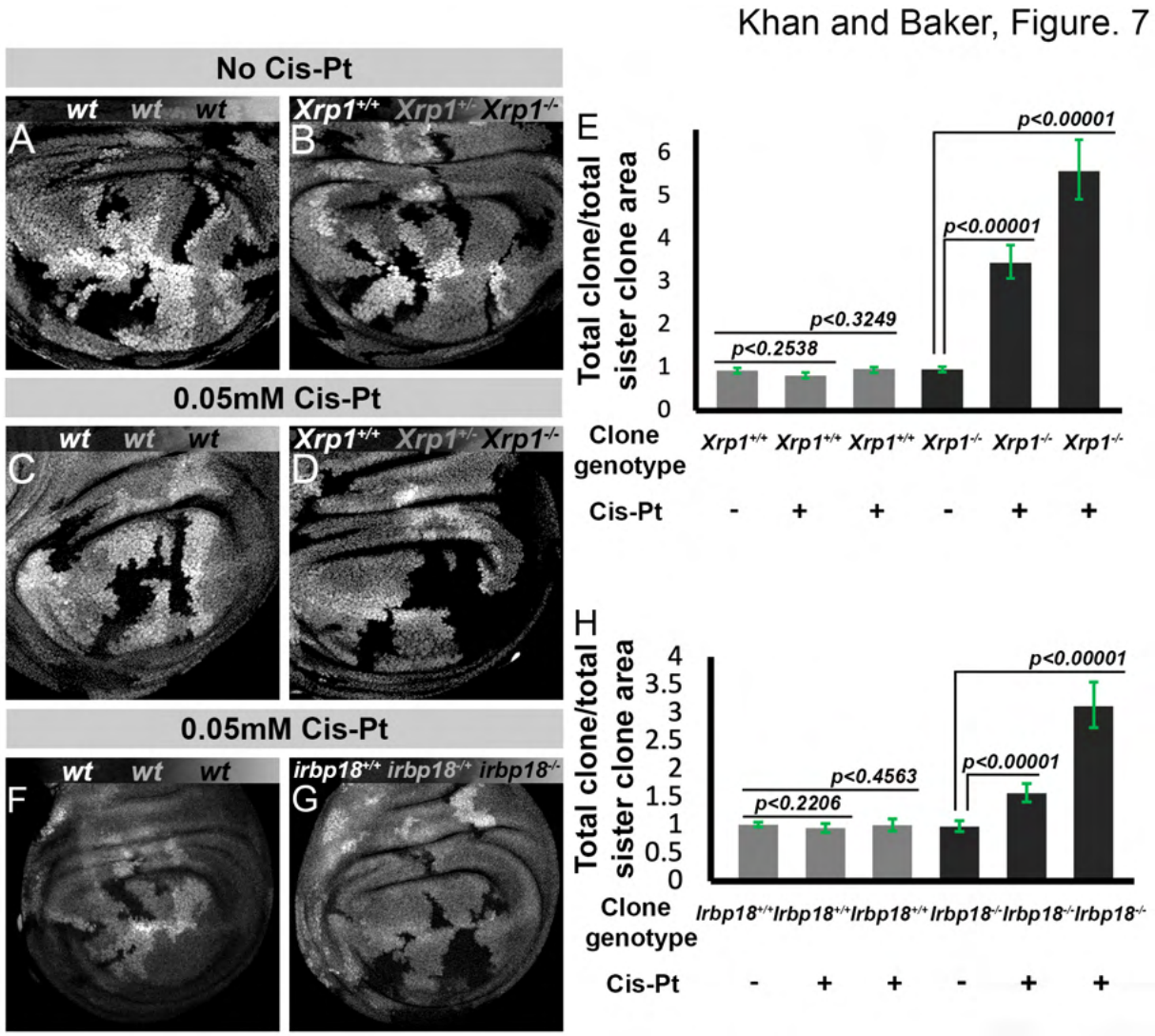

Figure 7: Lack of Xrp1/irbp18 facilitate growth of cells over wild type cells

(A-D) III instar wing imaginal disc stained for RFP, heterozygous cells one copy RFP (intermediate grey), sister clone with two copy of RFP (dark grey) and clone is marked

by absence of RFP (black) under control condition (no Cis-Pt) 72 hours after clonal induction (a.c.i) in *FRT82* (A), *FRT82Xrp1*$^{m2-73}$ (B) and 96 hours a.c.i + 0.05mM Cis-Pt treatment in *FRT82* (C) & *FRT82Xrp1*$^{m2-73}$ (D). (E) Total clone to total sister clone (*FRT82-RFP/82-RFP*) area measurements in individual discs, plotted as ratio at 72 hours a.c.i + no Cis-Pt, 72 hours and 96 hours after clonal induction + 0.05mM Cis-Pt treatment. (F-G) III instar wing imaginal disc stained for GFP, heterozygous cells one copy GFP (intermediate grey), sister clone with two copy of GFP (dark grey) and clone is marked by absence of GFP (black) 96 hours a.c.i + 0.05mM Cis-Pt treatment in *FRT80* (F) & *irbp18*$^{[f05006]}$ *FRT80* (G). (H) Total clone to total sister clone (*GFP-FRT80/80-GFP*) area measurements in individual discs, plotted as ratio at 72 hours a.c.i + no Cis-Pt, 72 hours and 96 a.c.i + 0.05mM Cis-Pt treatment. N= 10 discs each genotype, data is plotted as mean± SEM, two-tailed student t-test for independent sample was performed for statistical significance.

Figure 7 - source data file 1: Clone size quantification A-E

Figure 7 - source data file 2: Clone size quantification F-H

Genotype: (A & C) *p{hs:FLP}; FRT82-RFP/ FRT82* (30 min hs, 48 hr A.E.L), (B & D) *p{hs:FLP}; FRT82-RFP/ FRT82-Xrp1*$^{m2-73}$ (30 min hs, 48 hr A.E.L), (F) *p{hs:FLP}; GFP-FRT80/ irbp18*$^{[f05006]}$*-FRT80* (30 min hs, 48 hr A.E.L), (G) *p{hs:FLP}; GFP-FRT80/irbp18*$^{[f05006]}$*-FRT80* (30 min hs, 48 hr A.E.L)

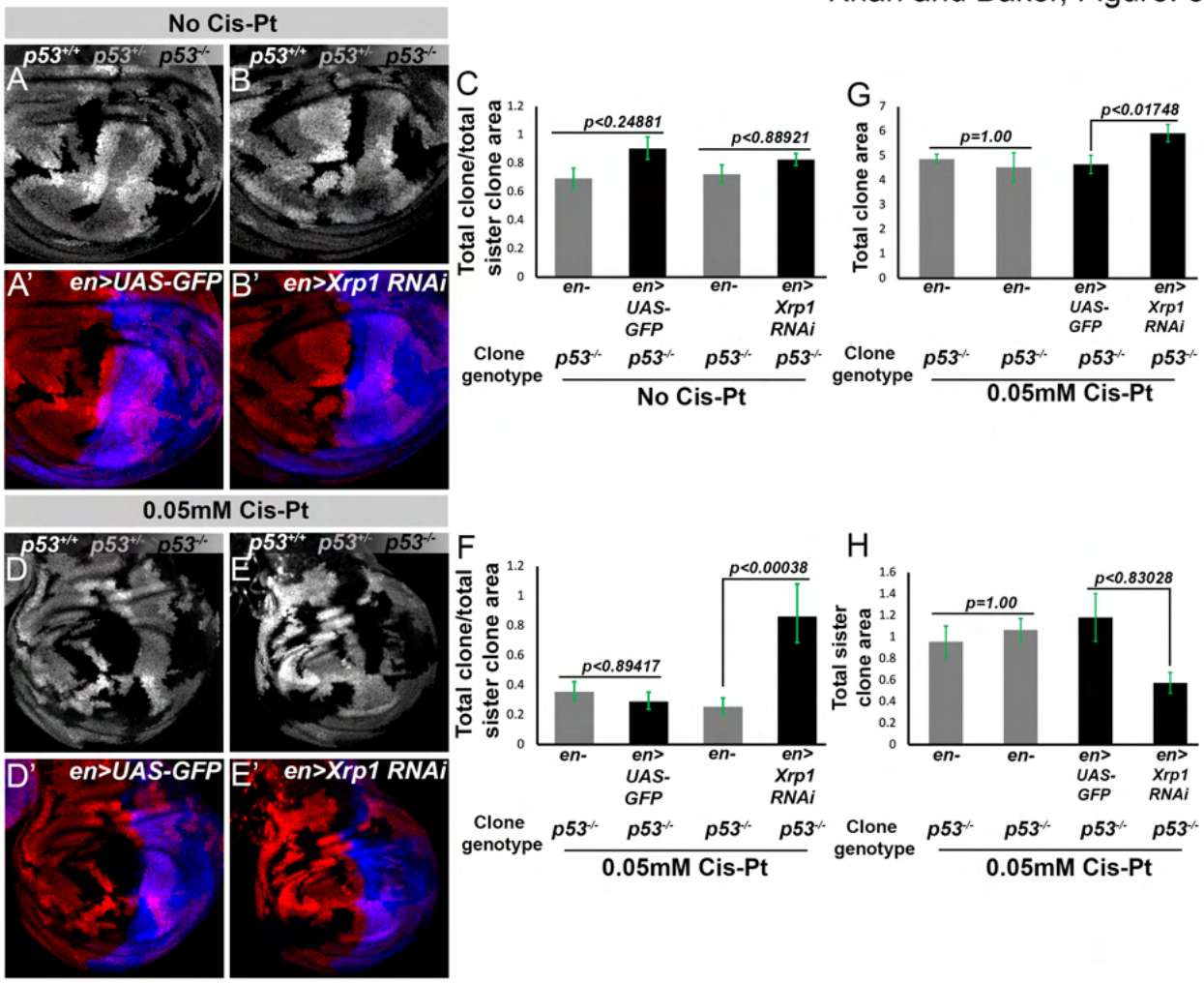

Figure 8: Lack of Xrp1 co-operates with *p53*$^{-/-}$ mutant cell expansion

(A-B) III instar wing imaginal disc stained for RFP, heterozygous cells one copy RFP (intermediate grey, dull red), sister clone with two copy of RFP (dark grey, bright red) and clone is marked by absence of RFP (black) and the engrailed compartment (blue). Image showing *p53*$^{-/-}$ mutant and *FRT82-RFP/82-RFP* clone 72 hours after clonal induction (a.c.i), comparing the total clone to sister clone area in anterior versus posterior compartment in control (*en-Gal4::UAS-GFP; FRT82-RFP/FRT82-p53*$^{[5A-1-4]}$) (A) and experimental (*en-Gal4::UAS-GFP, UAS-Xrp1 RNAi; FRT82-RFP/FRT82-p53*$^{[5A-1-4]}$) (B). (C) Quantification of the *p53*$^{-/-}$ mutant clone to sister clone (*FRT82-RFP/82-RFP*) area in anterior and posterior compartment from the data shown in (A) and (B). (D-E) Images showing *p53*$^{-/-}$ mutant and sister clone (*Frt82-RFP/82-RFP*) 96 hours a.c.i + 0.05mM Cis-Pt treatment, comparing the total clone to sister clone area in anterior versus posterior

1076 compartment in control (*en-Gal4::UAS-GFP;FRT82-RFP/FRT82-p53*$^{[5A-1-4]}$) (D) and
1077 experimental (*en-Gal4::UAS-GFP, UAS-Xrp1 RNAi; FRT82-RFP/FRT82-p53*$^{[5A-1-4]}$) (E). (F)
1078 Quantification of the *p53*$^{-/-}$ mutant clone to sister clone (*FRT82-RFP/82-RFP*) area in
1079 anterior and posterior compartment from the data shown in (D) and (E). (G) Total *p53*$^{-/-}$
1080 mutant clone area quantified in anterior and posterior compartment from Cis-Pt treated
1081 disc in control (*en-Gal4::UAS-GFP;FRT82-RFP/FRT82-p53*$^{[5A-1-4]}$) and experimental (*en-*
1082 *Gal4::UAS-GFP, UAS-Xrp1 RNAi;FRT82-RFP/FRT82-p53*$^{[5A-1-4]}$). (H) Total *p53*$^{-/-}$ mutant
1083 sister clone area quantified in anterior and posterior compartment from Cis-Pt treated
1084 disc in control (*en-Gal4::UAS-GFP;FRT82-RFP/FRT82-p53*$^{[5A-1-4]}$) and experimental (*en-*
1085 *Gal4::UAS-GFP, UAS-Xrp1 RNAi; FRT82-RFP/FRT82-p53*$^{[5A-1-4]}$). Statistics: (A-B, C) N= 12
1086 for each genotype, (D-E, F-G) N= 16 for each genotype, data is plotted as mean± SEM,
1087 One-way Anova with Bonferroni-Holm multiple comparison correction was performed
1088 for panel C and G-H, Holm p values are displayed on the graphs.
1089 Figure 8- source data file 1- clone area quantification A-H
1090
1091 Genotype: (A & D) *p{hs:FLP}; en-Gal4::UAS-GFP; FRT82-RFP/FRT82-p53*$^{[5A-1-4]}$ (30 min hs,
1092 48 hr A.E.L), (B & E) *p{hs:FLP}; en-Gal4::UAS-GFP, UAS-Xrp1 RNAi* (VDRC 107860);
1093 *FRT82-RFP/FRT82-p53*$^{[5A-1-4]}$ (30 min hs, 48 hr A.E.L)
1094

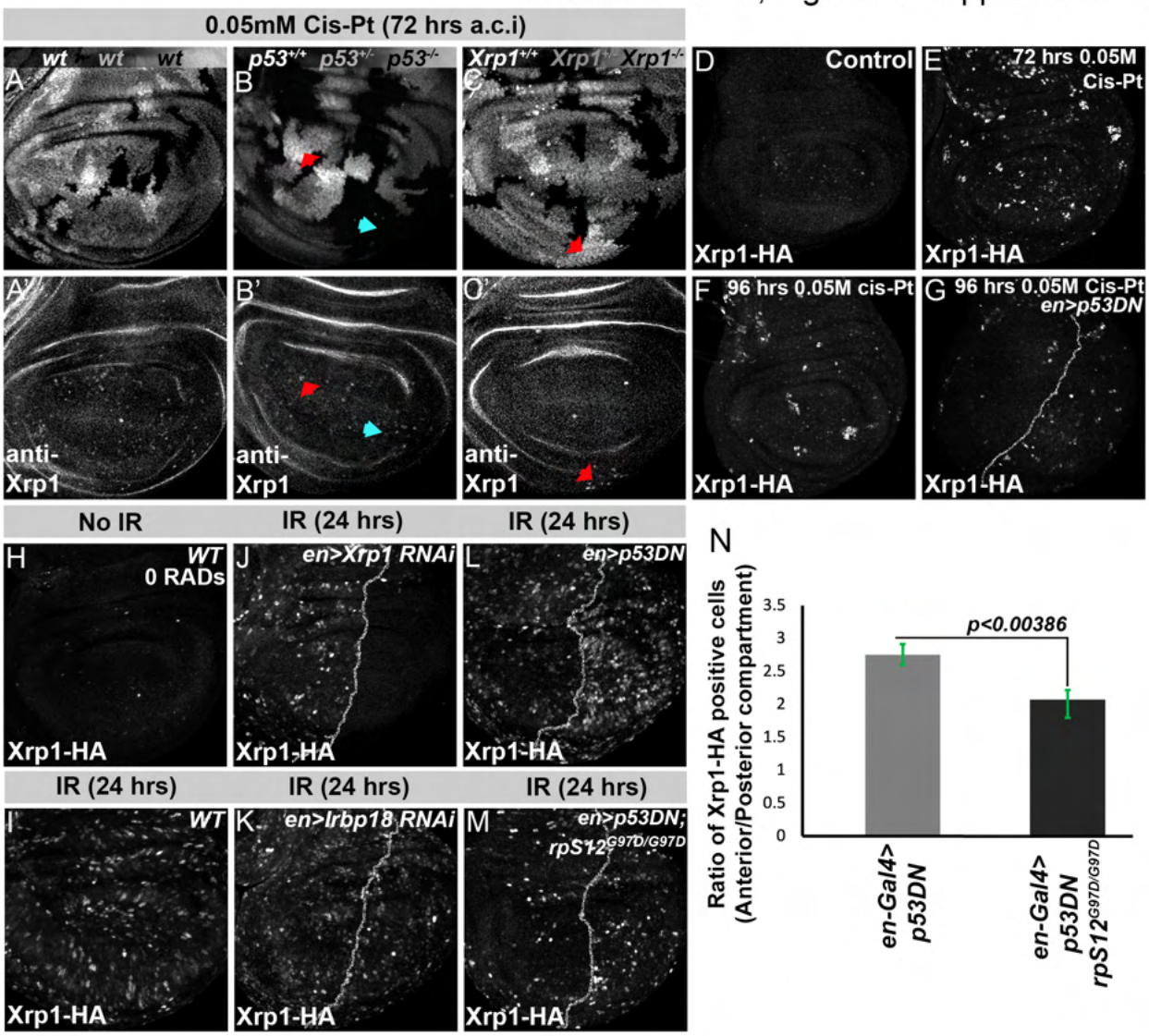

Figure 8- Supplemental 1: Xrp1 induction independent of p53

(A-C) III instar wing imaginal disc stained for RFP, heterozygous cells one copy RFP (intermediate grey), sister clone with two copy of RFP (dark grey) and clone is marked by absence of RFP (black) and stained for anti-Xrp1 (long isoform) in *FRT82* (A), *FRT82p53*$^{[5A-1-4]}$] (B) and *FRT82Xrp1*$^{m2-73}$ (C). (D-G) Xrp1-HA expression in control disc (D), 72 hours (E), 96 hours (F) and 96 hours in p53 dominant negative (*UAS-p53*^{H159N}) after 0.05mM Cis-Pt (G). (I-M) Xrp1-HA expression in control disc (H), 24 hours after 1500 rads (I), *UAS-Xrp1* RNAi (J), *UAS-Irbp1* RNAi (K), *UAS-p53*^{H159N} (L) and *UAS-p53*^{H159N} in *rpS12*$^{G97D/G97D}$ mutant background (M). (N) Ratio of Xrp1 positive cells in anterior to posterior compartment in *UAS-p53*^{H159N} and *UAS-p53*^{H159N} in *rpS12*$^{G97D/G97D}$ mutant

background. N= 8 for (L-N), data is plotted as mean± SEM, student t-test two-tailed for independent sample was performed for statistical significance.

Figure 8 – Supplemental 1- source data file 1: quantification for Xrp1-HA positive cells L-N

Genotype: (A) *p{hs:FLP}; FRT82-RFP/FRT82* (30 min hs, 48 hr A.E.L), (B) *p{hs:FLP}; FRT82-RFP/FRT82-p53*$^{[5A-1-4]}$ (30 min hs, 48 hr A.E.L), (C) *p{hs:FLP}; FRT82-RFP/FRT82-Xrp1*$^{m2-73}$(30 min hs, 48 hr A.E.L), (D-G) *Xrp1-HA*, (H & I) *Xrp1-HA*, (J) *en-Gal4::UAS-RFP; UAS-Xrp1 RNAi* (VDRC 107860)*; Xrp1-HA*, (K) *en-Gal4::UAS-RFP; UAS-Irbp18 RNAi; Xrp1-HA*, (L) *en-Gal4::UAS-RFP; UAS-p53DN*^{H159N} (Bl. 8420)*; Xrp1-HA*, (M) *en-Gal4::UAS-RFP; UAS-p53DN*^{H159N} (Bl. 8420)*; Xrp1-HA-rpS12*$^{G97D/G97D}$

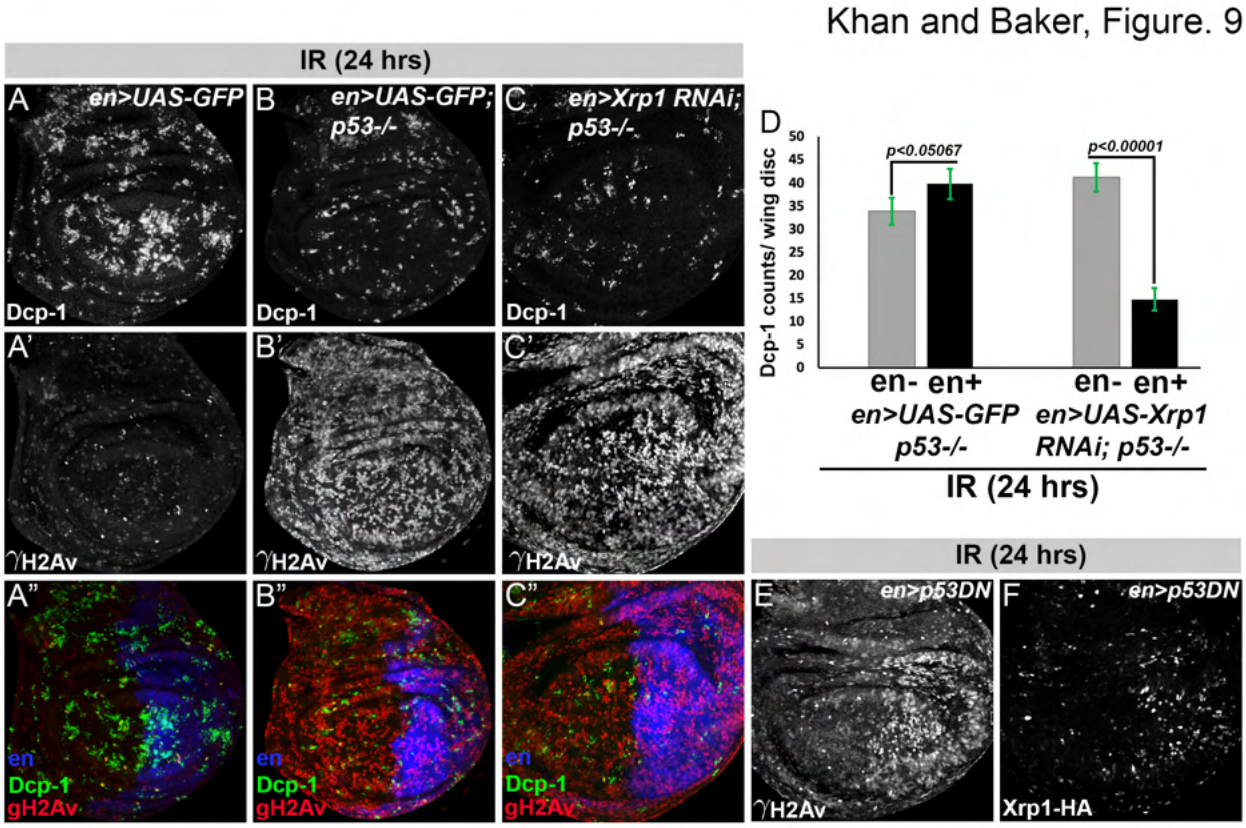

Figure 9: Xrp1 limits genomic instabilities by removing aneuploid cells in an p53-independent manner

(A-C) III instar wing disc from larvae dissected 24 hours after 1500 Rads of γ-rays treatment, stained for cell death (Dcp-1, green), DNA damage signaling (γH2Av, red) in

1123 control (*en-Gal4, UAS-GFP*) (A), *p53*$^{-/-}$ mutant (B) and Xrp1 k/d in *p53*$^{-/-}$ mutant
1124 background (C). (D) Quantification of Dcp-1 positive cells anterior versus posterior
1125 compartment in *p53*$^{-/-}$ mutant and Xrp1 k/d in *p53*$^{-/-}$ mutant background. (E) γH2Av and
1126 (F) Xrp1-HA levels 24 hours after irradiation in the posterior compartment of wing disc
1127 expressing *p53*^{H159N} under the control of engrailed Gal4. N= 15 for (A-D), data is plotted
1128 as mean± SEM, student t-test two-tailed for independent sample was performed for
1129 statistical significance. N= 8, for (E & F).
1130 Figure 9- source data file 1- Dcp-1 positive cell number quantification A-D
1131
1132 Genotype: Figure 9 (A) *en-Gal4::UAS-GFP; FRT82-RFP/FRT82-p53*$^{[5A-1-4]}$, (B) *en-Gal4::UAS-*
1133 *GFP; FRT82-RFP/FRT82-p53*$^{[5A-1-4]}$, (C) *en-Gal4::UAS-GFP, UAS-Xrp1 RNAi* (VDRC
1134 107860)*; FRT82-RFP/FRT82-p53*$^{[5A-1-4]}$
1135

Khan and Baker, Figure. 9- supplemental 1

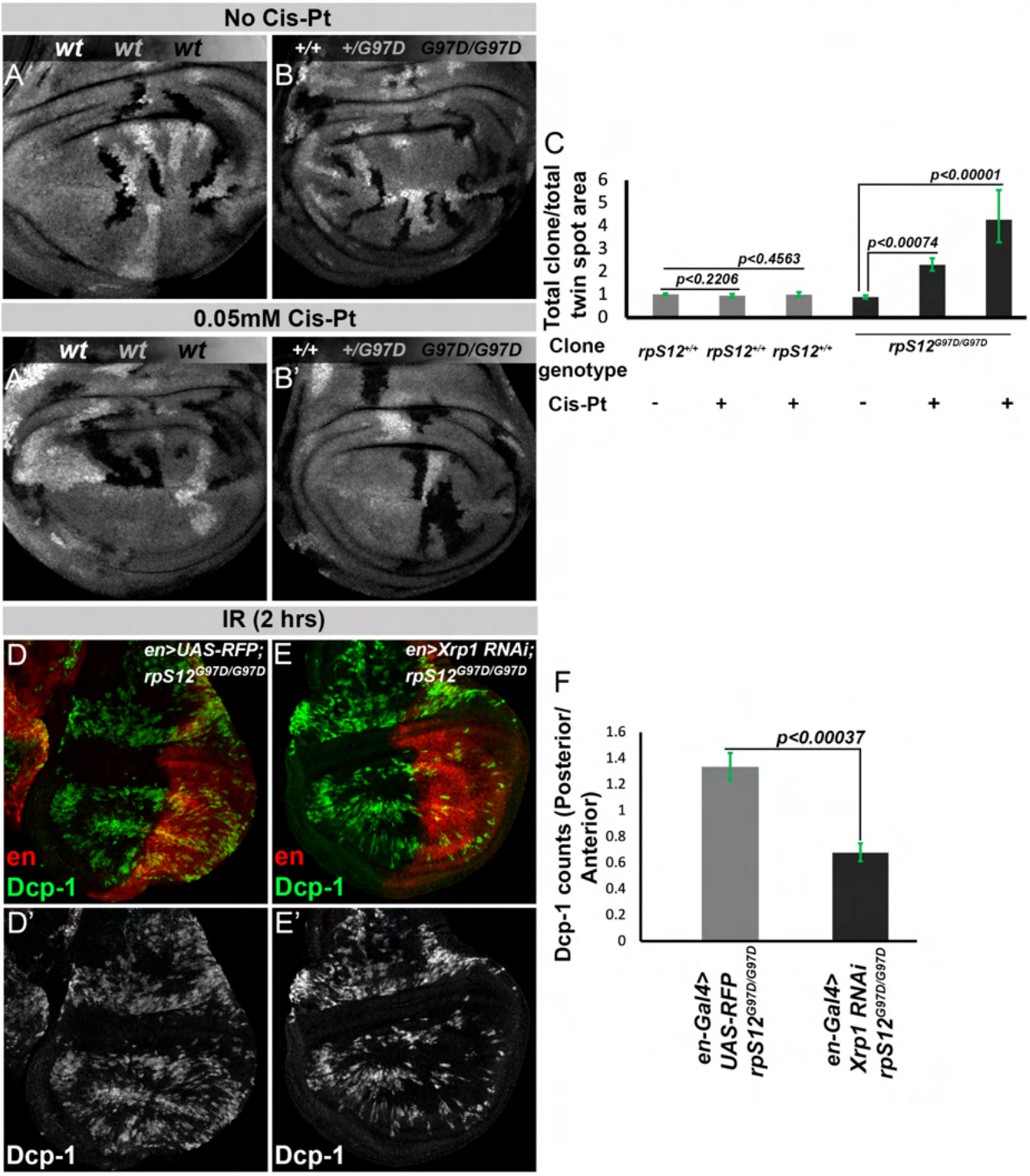

Figure 9- Supplemental 1: RpS12 remove aneuploid cells by cell competition created by chronic 0.05mM Cis-Pt treatment

(A-B) III instar wing imaginal disc stained for GFP, heterozygous cells one copy GFP (intermediate grey), sister clone with two copy of GFP (dark grey) and clone is marked by absence of GFP (black) 96 hours after clonal induction (a.c.i) + 0.05mM Cis-Pt

1142 treatment in *GFP-FRT80* (A) & *rpS12*^{G97D}*-FRT80* (B). (C) Total clone to total sister clone
1143 (*GFP-FRT80*/*GFP-FRT80*) area measurements in individual discs, plotted as ratio at 72
1144 hours a.c.i + no Cis-Pt, 72 hours and 96 hours a.c.i + 0.05mM Cis-Pt treatment. (D-F) Cell
1145 death measured by anti-Dcp-1 (green and gray scale) in wing imaginal discs dissected at
1146 2 hours after 1500 Rads, measured in en-Gal4 (posterior compartment (red)) versus
1147 anterior compartment *UAS-RFP; rpS12*^{G97D} (D), and *UAS-Xrp1 RNAi; rpS12*^{G97D} (E). Dcp-1
1148 positive cells were quantified in anterior and posterior compartment and plotted as the
1149 ratio of the number of Dcp-1 positive cells (F). N= 12 discs for (A-C), N= 6 discs for (D-
1150 F), data is plotted as mean± SEM, student t-test two-tailed for independent sample was
1151 performed for statistical significance.
1152 Figure 9 – Supplemental 1- source data file 1: Clone and sister area quantification A-C
1153 Figure 9 – Supplemental 1- source data file 2: Dcp-1 positive cell number quantification
1154 D-F
1155
1156 Genotype: (A) *p{hs:FLP}; GFP-FRT80/ FRT82* (30 min hs, 48 hr A.E.L), (B) *p{hs:FLP}; GFP-*
1157 *FRT80/rpS12*$^{G97D/G97D}$*-FRT80* (30 min hs, 48 hr A.E.L), (D) *en-Gal4::UAS-RFP; rpS12*$^{G97D/G97D}$,
1158 (E) *en-Gal4::UAS-RFP, UAS-Xrp1 RNAi* (VDRC 107860)*; rpS12*$^{G97D/G97D}$
1159
1160

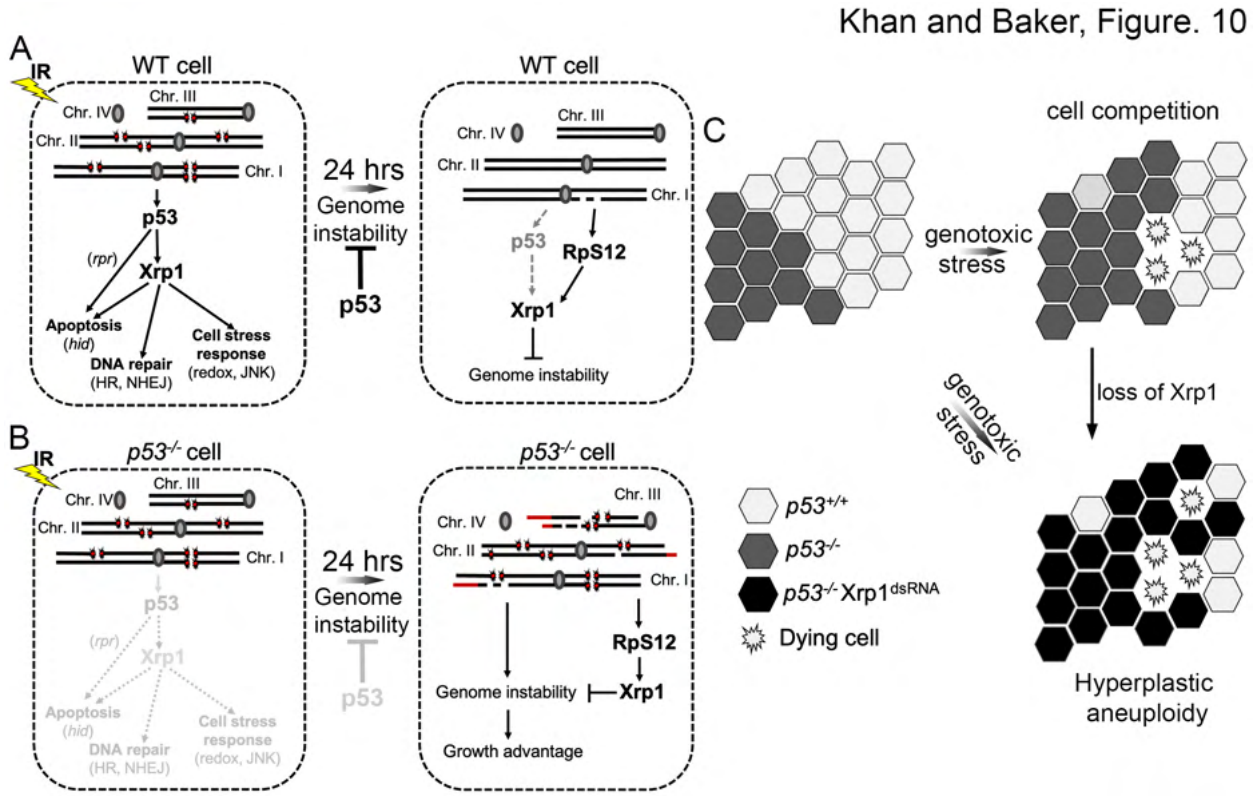

Figure 10: Model

(A) Wild type cells activate p53 in response to IR, p53 activate Xrp1 which in turn mediate many functions of p53 in DNA damage response. p53 via Xrp1 promote DNA repair, cell death to keep a check on accumulation of cells with abnormal genomic content. p53 strongly regulate cell death in comparison to Xrp1, which is important to remove damaged cells from the tissue, failure of which results in the accumulation of damaged cells that leads to compromised genomic integrity. Cells escaping p53-Xrp1 DDR are further removed by RpS12-Xrp1 dependent pathway that remove aneuploid cells via cell competition.

(B) Absence of p53, abrogates DDR (both DNA repair and cell death). Lack of DDR leads to build up of cells harboring abnormal genomic content (aneuploidy, chromosomal rearrangement, deletions). Persistence of such cells gives competitive growth advantage to *p53*$^{-/-}$ mutant cells. Part of this growth is opposed by p53-independent role of Xrp1 in removing aneuploid cells by cell competition. Simultaneous loss of both p53 and Xrp1 causes an additive by promoting persistence of damaged and aneuploid cells which in turn impart aggressive growth phenotype to the cells (hyperplastic aneuploidy).

(C) *p53*$^{-/-}$ mutant (dark grey cells) and *p53*$^{+/+}$ (light grey cells) cells grow to the same extent in unchallenged condition, *p53*$^{-/-}$ mutant cells gain competitive advantage over *p53*$^{+/+}$ cells upon treatment with genotoxin, the competitive growth advantage is further enhanced by simultaneous lack of both Xrp1 and p53 (black cells). We propose that the growth of p53 and Xrp1 double mutant cells is further promoted due to greater accumulation of cells with hyperplastic aneuploidies (black cells).

1208 **Supplementary Table 1:** Key Resources Table

Key Resources Table				
Reagent type (species) or resource	**Designation**	**Source or reference**	**Identifiers**	**Additional information**
gene (*Drosophila melanogaster*)	Xrp1		FLYBASE: FBgn0261113	
gene (*Drosophila melanogaster*)	irbp18		FLYBASE: FBgn0036126	
genetic reagent (*D. melanogaster*)	p53		FLYBASE: FBgn0039044	
genetic reagent (*D. melanogaster*)	rpS12		FLYBASE: FBgn0286213	
genetic reagent (*D. melanogaster*)	*Xrp1*$^{m2\text{-}73}$	(Lee et al. 2016)	FLYBASE: FBal0346068	Bloomington Drosophila Stock Center #81270
genetic reagent (*D. melanogaster*)	*Xrp1*^{02515}	(Spradling et al. 1999)	FLYBASE: FBal0009448	Bloomington Drosophila Stock Center #11569
genetic reagent (*D. melanogaster*)	*Xrp1*$^{attP\ flox}$	(Blanco, Cooper, and Baker 2020)		Strain maintained in Dr. Nicholas Baker's lab

genetic reagent (*D. melanogaster*)	Xrp1^{HA}	(Blanco, Cooper, and Baker 2020)		Strain maintained in Dr. Nicholas Baker's lab
genetic reagent (*D. melanogaster*)	UAS-Xrp1 (long isoform)	(Tsurui-Nishimura et al. 2013)	FLYBASE: FBal0284387	
genetic reagent (*D. melanogaster*)	*irbp18*^{05006}	(Francis et al. 2016)	FLYBASE: FBal0185260	Exelisis Drosophila Collection #f05006
genetic reagent (*D. melanogaster*)	*rpS12*^{G97D}		FLYBASE: FBgn0286213	Strain maintained in Dr. Nicholas Baker's lab
genetic reagent (*D. melanogaster*)	*p53*$^{[5A-1-4]}$		FLYBASE: FBgn0039044	Bloomington Drosophila Stock Center #6815
genetic reagent (*D. melanogaster*)	UAS-p53.H159N.Ex-2 (Chr. II)		FLYBASE: FBti0040583	Bloomington Drosophila Stock Center #8420
genetic reagent (*D. melanogaster*)	UAS-p53.H159N.Ex -3 (Chr. III)		FLYBASE: FBti0040584	Bloomington Drosophila Stock Center #8421
genetic reagent (*D. melanogaster*)	UAS-dsRNA^{Xrp1}	(Ni et al. 2011)	FLYBASE: FBti0144696	Bloomington Drosophila Stock Center #34521
genetic reagent (*D. melanogaster*)	UAS-dsRNA^{Xrp1}		FLYBASE: FBst0479673	Vienna Drosophila Resource

				Center #107860
genetic reagent (*D. melanogaster*)	UAS-dsRNA^{irbp18}	(Ni et al. 2011)	FLYBASE: FBti0140125	Bloomington Drosophila Stock Center #33652
genetic reagent (*D. melanogaster*)	UAS-dsRNA^{w}	(Ni et al. 2011)	FLYBASE: FBtp0064645	Bloomington Drosophila Stock Center #33623
genetic reagent (*D. melanogaster*)	arm-LacZ	(Vincent, Girdham, and O'Farrell 1994)	FLYBASE: FBal0040819	
genetic reagent (*D. melanogaster*)	Ubi-GFP	(Davis, O'Farrell, and Girdham 1995)	FLYBASE: FBal0047085	
genetic reagent (*D. melanogaster*)	M(2)56F (mutating RpS18)	Laboratory of Y. Hiromi	FLYBASE: FBal0011916	
genetic reagent (*D. melanogaster*)	hs-FLP	(Struhl and Basler 1993)	FLYBASE: FBtp0001101	
genetic reagent (*D. melanogaster*)	ey-FLP	(Newsome, Åsling, and Dickson 2000)	FLYBASE: FBal0098303	
genetic reagent (*D. melanogaster*)	GMR-gal4	(Freeman 1996)	FLYBASE: FBtp0001315	
genetic reagent (*D. melanogaster*)	P{neoFRT}42 D	(Xu and Rubin 1993)	FLYBASE: FBti0141188	Bloomington Drosophila Stock Center #1802

genetic reagent (*D. melanogaster*)	P{neoFRT}80B	(Xu and Rubin 1993)	FLYBASE: FBti0002073	Bloomington Drosophila Stock Center #1988
genetic reagent (*D. melanogaster*)	P{neoFRT}82B	(Xu and Rubin 1993)	FLYBASE: FBti0002074	Bloomington Drosophila Stock Center #2050, 2051
Antibody	Polyclonal Rabbit anti-XRP1 (short isoform)	(Francis et al. 2016)		1:200 dilution
Antibody	Mouse anti-HA Tag monoclonal	Cell Signalling Technology	Cat #2367 RRID:AB_10691311	1:100 dilution
Antibody	Mouse anti-beta galactosidase (mAb40-1a) monoclonal	DSHB	RRID: AB_2314509	1:100 dilution
Antibody	Rabbit anti-active-Dcp1 polyclonal	Cell Signalling Technology	Cat #9578 RRID:AB_2721060	1:50 dilution
Antibody	Mouse anti-p53 (25F4) monoclonal	DSHB	RRID: AB_579787	1:20 dilution

1220 REFERENCES

1221 Akdemir, F., A. Christich, N. Sogame, J. Chapo, and J. M. Abrams. 2007. "P53 Directs Focused
1222 Genomic Responses in Drosophila." *Oncogene* 26 (36): 5184–93.
1223 https://doi.org/10.1038/sj.onc.1210328.
1224 Allen, Mary Ann, Zdenek Andrysik, Veronica L Dengler, Hestia S Mellert, Anna Guarnieri, Justin A
1225 Freeman, Kelly D Sullivan, et al. 2014. "Global Analysis of P53-Regulated Transcription
1226 Identifies Its Direct Targets and Unexpected Regulatory Mechanisms." *ELife* 3 (May).
1227 https://doi.org/10.7554/elife.02200.
1228 Alpar, Lale, Cora Bergantiños, and Laura A. Johnston. 2018. "Spatially Restricted Regulation of
1229 Spätzle/Toll Signaling during Cell Competition." *Developmental Cell* 46 (6): 706-719.e5.
1230 https://doi.org/10.1016/j.devcel.2018.08.001.
1231 Andrysik, Zdenek, Matthew D. Galbraith, Anna L. Guarnieri, Sara Zaccara, Kelly D. Sullivan,
1232 Ahwan Pandey, Morgan MacBeth, Alberto Inga, and Joaquín M. Espinosa. 2017.
1233 "Identification of a Core TP53 Transcriptional Program with Highly Distributed Tumor
1234 Suppressive Activity." *Genome Research* 27 (10): 1645–57.
1235 https://doi.org/10.1101/gr.220533.117.
1236 Baillon, Ludovic, Federico Germani, R Claudia, Jochen Hilchenbach, and Konrad Basler. 2018.
1237 "Xrp1 Is a Transcription Factor Required for Cell Competition-Driven Elimination of Loser
1238 Cells." *Scientific Report*, no. July: 1–10. https://doi.org/10.1038/s41598-018-36277-4.
1239 Baker, N E. 2017. "Mechanisms of Cell Competition Emerging from Drosophila Studies." *Current*
1240 *Opinion in Cell Biology* 48: 40–46. https://doi.org/10.1016/j.ceb.2017.05.002.
1241 Baker, Fang Jin, Karthik B. Jeganathan, and Jan M. van Deursen. 2009. "Whole Chromosome
1242 Instability Caused by Bub1 Insufficiency Drives Tumorigenesis through Tumor Suppressor
1243 Gene Loss of Heterozygosity." *Cancer Cell* 16 (6): 475–86.
1244 https://doi.org/10.1016/j.ccr.2009.10.023.
1245 Baker, N E. 2020. "Emerging Mechanisms of Cell Competition." *Nature Reviews Genetics* 21
1246 (11): 683–97. https://doi.org/10.1038/s41576-020-0262-8.
1247 Baker, N.E., M. Kiparaki, and C. Khan. 2019. "A Potential Link between P53, Cell Competition
1248 and Ribosomopathy in Mammals and in Drosophila." *Developmental Biology* 446 (1).
1249 https://doi.org/10.1016/j.ydbio.2018.11.018.
1250 Blanco, Jorge, Jacob C. Cooper, and Nicholas E. Baker. 2020. "Roles of C/EBP Class BZip Proteins
1251 in the Growth and Cell Competition of Rp ('Minute') Mutants in Drosophila." *ELife* 9: 1–27.
1252 https://doi.org/10.7554/eLife.50535.
1253 Bondar, Tanya, and Ruslan Medzhitov. 2010. "P53-Mediated Hematopoietic Stem and
1254 Progenitor Cell Competition." *Cell Stem Cell* 6 (4): 309–22.
1255 https://doi.org/10.1016/j.stem.2010.03.002.
1256 Brennan, Christopher M., Laura Pontano Vaites, Jonathan N. Wells, Stefano Santaguida, Joao A.
1257 Paulo, Zuzana Storchova, J. Wade Harper, Joseph A. Marsh, and Angelika Amon. 2019.
1258 "Protein Aggregation Mediates Stoichiometry of Protein Complexes in Aneuploid Cells."
1259 *Genes and Development* 33 (15–16): 1031–47. https://doi.org/10.1101/gad.327494.119.
1260 Brodsky, M H, W Nordstrom, G Tsang, E Kwan, G M Rubin, and J M Abrams. 2000. "Drosophila
1261 P53 Binds a Damage Response Element at the Reaper Locus." *Cell* 101: 103–13.
1262 https://doi.org/10.1016/S0092-8674(00)80627-3.

1263 Brodsky, M H, Brian T. Weinert, Garson Tsang, Yikang S. Rong, Nadine M. McGinnis, Kent G.
1264 Golic, Donald C. Rio, and Gerald M. Rubin. 2004. "Drosophila Melanogaster MNK/Chk2 and
1265 P53 Regulate Multiple DNA Repair and Apoptotic Pathways Following DNA Damage."
1266 *Molecular and Cellular Biology* 24 (3): 1219–31. https://doi.org/10.1128/mcb.24.3.1219-
1267 1231.2004.
1268 Brown, Brian, Sahana Mitra, Finnegan D Roach, Deepika Vasudevan, and Hyung Don Ryoo.
1269 2021. "The Transcription Factor Xrp1 Is Required for PERK-Mediated Antioxidant Gene
1270 Induction in Drosophila." *ELife* 10: 74047. https://doi.org/10.7554/eLife.
1271 Brumby, A.M., and H.E. Richardson. 2003. "Scribblemutants Cooperate with Oncogenic Ras or
1272 Notch to Cause Neoplastic Overgrowth in Drosophila." *The EMBO Journal* 22: 5769–79.
1273 Bursac, Sladana, Maja Cokaric, Giulio Donati, and Sinisa Volarevic. 2014. "Activation of the
1274 Tumor Suppressor P53 upon Impairment of Ribosome Biogenesis." *BBA - Molecular Basis*
1275 *of Disease* 1842 (6): 817–30. https://doi.org/10.1016/j.bbadis.2013.08.014.
1276 Chakraborty, Riddhita, Ying Li, Lei Zhou, and Kent G. Golic. 2015. "Corp Regulates P53 in
1277 Drosophila Melanogaster via a Negative Feedback Loop." *PLoS Genetics* 11 (7): 1–25.
1278 https://doi.org/10.1371/journal.pgen.1005400.
1279 Chakravarti, Ananya, Heshani N. Thirimanne, Savanna Brown, and Brian R. Calvi. 2022.
1280 "Drosophila P53 Isoforms Have Overlapping and Distinct Functions in Germline Genome
1281 Integrity and Oocyte Quality Control." *ELife* 11 (January).
1282 https://doi.org/10.7554/eLife.61389.
1283 Chen, Jiandong. 2016. "The Cell-Cycle Arrest and Apoptotic Functions of P53 in Tumor Initiation
1284 and Progression." *Cold Spring Harbor Perspectives in Medicine* 6 (3).
1285 https://doi.org/10.1101/cshperspect.a026104.
1286 Christophorou, M. A., I. Ringshausen, A. J. Finch, L. Brown Swigart, and G. I. Evan. 2006. "The
1287 Pathological Response to DNA Damage Does Not Contribute to P53-Mediated Tumour
1288 Suppression." *Nature* 443 (7108): 214–17. https://doi.org/10.1038/nature05077.
1289 Christophorou, Maria A., Dionisio Martin-Zanca, Laura Soucek, Elizabeth R. Lawlor, Lamorna
1290 Brown-Swigart, Emmy W. Verschuren, and Gerard I. Evan. 2005. "Temporal Dissection of
1291 P53 Function in Vitro and in Vivo." *Nature Genetics* 37 (7): 718–26.
1292 https://doi.org/10.1038/ng1572.
1293 Clemente-Ruiz, Marta, and Marco Milán. 2015. "Epithelial Cell Division: Keeping Aneuploidy
1294 Levels in Check." *Current Biology*. Cell Press. https://doi.org/10.1016/j.cub.2015.02.008.
1295 Dasari, Shaloam, and Paul Bernard Tchounwou. 2014. "Cisplatin in Cancer Therapy: Molecular
1296 Mechanisms of Action." *European Journal of Pharmacology* 740: 364–78.
1297 https://doi.org/https://doi.org/10.1016/j.ejphar.2014.07.025.
1298 Davis, Ilan, Patrick H. O'Farrell, and Charles, H. Girdham. 1995. "A Nuclear GFP That Marks
1299 Nuclei in Living Drosophila Embryos; Maternal Supply Overcomes a Delay in the
1300 Appearance of Zygotic Fluorescence." *Developmental Biology* 170 (2): 726–29.
1301 Dekanty, A., L. Barrio, and M. Milán. 2015. "Contributions of DNA Repair, Cell Cycle Checkpoints
1302 and Cell Death to Suppressing the DNA Damage-Induced Tumorigenic Behavior of
1303 Drosophila Epithelial Cells." *Oncogene* 34 (8): 978–85.
1304 https://doi.org/10.1038/onc.2014.42.
1305 Dekanty, A., Lara Barrio, Mariana Muzzopappa, Herbert Auer, and Marco Milán. 2012.
1306 "Aneuploidy-Induced Delaminating Cells Drive Tumorigenesis in Drosophila Epithelia."

1307 *Proceedings of the National Academy of Sciences of the United States of America* 109 (50):
1308 20549–54. https://doi.org/10.1073/pnas.1206675109.
1309 Donati, G, S Bertoni, E Brighenti, M Vici, Trere´1 Trere´1, S Volarevic, L Montanaro, and M
1310 Derenzini. 2011. "The Balance between RRNA and Ribosomal Protein Synthesis Up- and
1311 Downregulates the Tumour Suppressor P53 in Mammalian Cells." *Oncogene* 30: 3274–88.
1312 https://doi.org/10.1038/onc.2011.48.
1313 Fan, Y, T v Lee, D Xu, Z Chen, a-F Lamblin, H Steller, and a Bergmann. 2010. "Dual Roles of
1314 Drosophila P53 in Cell Death and Cell Differentiation." *Cell Death and Differentiation* 17
1315 (6): 912–21. https://doi.org/10.1038/cdd.2009.182.
1316 Fernandez-Antoran, David, Gabriel Piedrafita, Kasumi Murai, Swee Hoe Ong, Albert Herms,
1317 Christian Frezza, and Philip H. Jones. 2019. "Outcompeting P53-Mutant Cells in the Normal
1318 Esophagus by Redox Manipulation." *Cell Stem Cell* 25 (3): 329-341.e6.
1319 https://doi.org/10.1016/j.stem.2019.06.011.
1320 Fischer, M. 2017. "Census and Evaluation of P53 Target Genes." *Oncogene* 36 (28): 3943–56.
1321 https://doi.org/10.1038/onc.2016.502.
1322 Foijer, Floris, Viji M. Draviam, and Peter K. Sorger. 2008. "Studying Chromosome Instability in
1323 the Mouse." *Biochimica et Biophysica Acta - Reviews on Cancer*.
1324 https://doi.org/10.1016/j.bbcan.2008.07.004.
1325 Francis, Malik Joseph, Siobhan Roche, Michael Jeffrey Cho, Eileen Beall, Bosun Min, Ronaldo
1326 Paolo Panganiban, and Donald C. Rio. 2016. "Drosophila IRBP BZIP Heterodimer Binds P-
1327 Element DNA and Affects Hybrid Dysgenesis." *Proceedings of the National Academy of*
1328 *Sciences of the United States of America* 113 (46): 13003–8.
1329 https://doi.org/10.1073/pnas.1613508113.
1330 Freeman, Matthew. 1996. "Reiterative Use of the EGF Receptor Triggers Differentiation of All
1331 Cell Types in the Drosophila Eye." *Cell*. Vol. 87.
1332 García-Castillo, Herbert, Ana Isabel Vásquez-Velásquez, Horacio Rivera, and Patricio Barros-
1333 Núñez. 2008. "Clinical and Genetic Heterogeneity in Patients with Mosaic Variegated
1334 Aneuploidy: Delineation of Clinical Subtypes." *American Journal of Medical Genetics, Part*
1335 *A* 146 (13): 1687–95. https://doi.org/10.1002/ajmg.a.32315.
1336 Gogna, Rajan, and Eduardo Moreno. 2020. "Emerging Role of Cell Competition in Cancer."
1337 *Seminars in Cancer Biology*. Academic Press.
1338 https://doi.org/10.1016/j.semcancer.2020.04.005.
1339 Hanks, Sandra, Kim Coleman, Sarah Reid, Alberto Plaja, Helen Firth, David FitzPatrick, Alexa
1340 Kidd, et al. 2004. "Constitutional Aneuploidy and Cancer Predisposition Caused by Biallelic
1341 Mutations in BUB1B." *Nature Genetics* 36 (11): 1159–61. https://doi.org/10.1038/ng1449.
1342 Igaki, Tatsushi, Raymond A. Pagliarini, and Tian Xu. 2006. "Loss of Cell Polarity Drives Tumor
1343 Growth and Invasion through JNK Activation in Drosophila." *Current Biology* 16 (11): 1139–
1344 46. https://doi.org/10.1016/j.cub.2006.04.042.
1345 Jean-Paul Vincent, Chaeles H. Girdham, and Patrick H. O'Farrell. 1994. "A Cell-Autonomous,
1346 Ubiquitous Marker for the Analysis of Drosophila Genetic Mosaics." *Developmental Biology*
1347 164: 328–31.
1348 Ji, Zhejun, Jacky Chuen, Marianthi Kiparaki, and Nicholas Baker. 2021. "Cell Competition
1349 Removes Segmental Aneuploid Cells from Drosophila Imaginal Disc-Derived Tissues Based
1350 on Ribosomal Protein Gene Dose." *ELife* 10 (April). https://doi.org/10.7554/eLife.61172.

1351 Ji, Zhejun, Marianthi Kiparaki, Virginia Folgado, Amit Kumar, Jorge Blanco, Gerard Rimesso,
1352 Jacky Chuen, Yang Liu, Deyou Zheng, and Nicholas E. Baker. 2019. "Drosophila RpS12
1353 Controls Translation, Growth, and Cell Competition through Xrp1." *PLoS Genetics* 15 (12).
1354 https://doi.org/10.1371/journal.pgen.1008513.
1355 Jin, Shengkan, Sebastian Martinek, Woo S Joo, Jennifer R Wortman, Nebojsa Mirkovic, Andrej
1356 Sali, Mark D Yandell, Nikola P Pavletich, Michael W Young, and Arnold J Levine. 2000.
1357 "Identification and Characterization of a P53 Homologue in Drosophila Melanogaster" 97
1358 (13).
1359 Joy, Jery, Lara Barrio, Celia Santos-Tapia, Daniela Romão, Nikolaos Nikiforos Giakoumakis,
1360 Marta Clemente-Ruiz, and Marco Milán. 2021. "Proteostasis Failure and Mitochondrial
1361 Dysfunction Leads to Aneuploidy-Induced Senescence." *Developmental Cell* 56 (14): 2043-
1362 2058.e7. https://doi.org/10.1016/j.devcel.2021.06.009.
1363 Kaiser, Alyssa M., and Laura D. Attardi. 2018. "Deconstructing Networks of P53-Mediated
1364 Tumor Suppression in Vivo." *Cell Death and Differentiation* 25 (1): 93–103.
1365 https://doi.org/10.1038/cdd.2017.171.
1366 Kale, Zhejun Ji, Marianthi Kiparaki, Jorge Blanco, Gerard Rimesso, Stephane Flibotte, and
1367 Nicholas E Baker. 2018. "Ribosomal Protein S12e Has a Distinct Function in Cell
1368 Competition." *Developmental Cell* 44 (1): 42–55.
1369 https://doi.org/10.1016/j.devcel.2017.12.007.
1370 Kale, W Li, C. H. Lee, and N E Baker. 2015. "Apoptotic Mechanisms during Competition of
1371 Ribosomal Protein Mutant Cells: Roles of the Initiator Caspases Dronc and Dream/Strica."
1372 *Cell Death and Differentiation* 22 (8): 1300–1312. https://doi.org/10.1038/cdd.2014.218.
1373 Kanda, Hiroshi, and Tatsushi Igaki. 2020. "Mechanism of Tumor-Suppressive Cell Competition in
1374 Flies." *Cancer Science* 111 (10): 3409–15. https://doi.org/10.1111/cas.14575.
1375 Kastenhuber, Edward R., and Scott W. Lowe. 2017. "Putting P53 in Context." *Cell* 170 (6): 1062–
1376 78. https://doi.org/10.1016/j.cell.2017.08.028.
1377 Khan, C., S. Muliyil, C. Ayyub, and B.J. Rao. 2017. "The Initiator Caspase Dronc Plays a Non-
1378 Apoptotic Role in Promoting DNA Damage Signalling in D. Melanogaster." *Journal of Cell*
1379 *Science* 130 (18). https://doi.org/10.1242/jcs.200782.
1380 Kiparaki, Marianthi, Chaitali Khan, Virginia Folgado-Marco, Jacky Chuen, Panagiotis Moulos, and
1381 Nicholas E Baker. 2022. "The Transcription Factor Xrp1 Orchestrates Both Reduced
1382 Translation and Cell Competition upon Defective Ribosome Assembly or Function." *ELife*
1383 11 (February). https://doi.org/10.7554/elife.71705.
1384 Kurtz, Paula, Amanda E. Jones, Bhavana Tiwari, Nichole Link, Annika Wylie, Charles Tracy,
1385 Helmut Krämer, and John M. Abrams. 2019. "Drosophila P53 Directs Nonapoptotic
1386 Programs in Postmitotic Tissue." *Molecular Biology of the Cell* 30 (11): 1339–51.
1387 https://doi.org/10.1091/mbc.E18-12-0791.
1388 La Cova, Claire de, Mauricio Abril, Paola Bellosta, Peter Gallant, and Laura A. Johnston. 2004.
1389 "Drosophila Myc Regulates Organ Size by Inducing Cell Competition." *Cell* 117 (1): 107–16.
1390 https://doi.org/10.1016/S0092-8674(04)00214-4.
1391 La Cova, Claire de, Nanami Senoo-Matsuda, Marcello Ziosi, D. Christine Wu, Paola Bellosta,
1392 Catarina M. Quinzii, and Laura A. Johnston. 2014. "Supercompetitor Status of Drosophila
1393 Myc Cells Requires P53 as a Fitness Sensor to Reprogram Metabolism and Promote
1394 Viability." *Cell Metabolism* 19 (3): 470–83. https://doi.org/10.1016/j.cmet.2014.01.012.

1395 Lacroix, Matthieu, Romain Riscal, Giuseppe Arena, Laetitia Karine Linares, and Laurent le Cam.
1396 2020. “Metabolic Functions of the Tumor Suppressor P53: Implications in Normal
1397 Physiology, Metabolic Disorders, and Cancer.” *Molecular Metabolism*. Elsevier GmbH.
1398 https://doi.org/10.1016/j.molmet.2019.10.002.
1399 Langton, Paul F., Michael E. Baumgartner, Remi Logeay, and Eugenia Piddini. 2021. “Xrp1 and
1400 Irbp18 Trigger a Feed-Forward Loop of Proteotoxic Stress to Induce the Loser Status.”
1401 Edited by Norbert Perrimon. *PLOS Genetics* 17 (12): e1009946.
1402 https://doi.org/10.1371/journal.pgen.1009946.
1403 Lee, C.-H., G. Rimesso, D. M. Reynolds, J. Cai, and N. E. Baker. 2016. “Whole-Genome
1404 Sequencing and IPLEX MassARRAY Genotyping Map an EMS-Induced Mutation Affecting
1405 Cell Competition in Drosophila Melanogaster.” *G3:Genes|Genomes|Genetics* 6 (October):
1406 3207–17. https://doi.org/10.1534/g3.116.029421.
1407 Lee, Marianthi Kiparaki, Jorge Blanco, Virginia Folgado, Zhejun Ji, Amit Kumar, Gerard Rimesso,
1408 and Nicholas E. Baker. 2018. “A Regulatory Response to Ribosomal Protein Mutations
1409 Controls Translation, Growth, and Cell Competition.” *Developmental Cell*, 1–14.
1410 https://doi.org/10.1016/j.devcel.2018.07.003.
1411 Levine, a J, W Hu, and Z Feng. 2006. “The P53 Pathway: What Questions Remain to Be
1412 Explored?” *Cell Death and Differentiation* 13 (6): 1027–36.
1413 https://doi.org/10.1038/sj.cdd.4401910.
1414 Li, Tongyuan, Ning Kon, Le Jiang, Minjia Tan, Thomas Ludwig, Yingming Zhao, Richard Baer, and
1415 Wei Gu. 2012. “Tumor Suppression in the Absence of P53-Mediated Cell-Cycle Arrest,
1416 Apoptosis, and Senescence.” *Cell* 149 (6): 1269–83.
1417 https://doi.org/10.1016/j.cell.2012.04.026.
1418 Li, Chenxi Wu, Xiang Ding, Wenzhe Li, and Lei Xue. 2020. “Toll Signaling Promotes JNK-
1419 Dependent Apoptosis in Drosophila.” *Cell Division* 15 (1). https://doi.org/10.1186/s13008-
1420 020-00062-5.
1421 Madigan, James P, Heather L Chotkowski, and Robert L Glaser. 2002. “DNA Double-Strand
1422 Break-Induced Phosphorylation of Drosophila Histone Variant H2Av Helps Prevent
1423 Radiation-Induced Apoptosis.” *Nucleic Acids Research* 30 (17): 3698–3705.
1424 https://doi.org/10.1093/nar/gkf496.
1425 Marusyk, Andriy, Christopher C. Porter, Vadym Zaberezhnyy, and James DeGregori. 2010.
1426 “Irradiation Selects for P53-Deficient Hematopoietic Progenitors.” *PLoS Biology* 8 (3).
1427 https://doi.org/10.1371/journal.pbio.1000324.
1428 Maruyama, Takeshi, and Yasuyuki Fujita. 2017. “Cell Competition in Mammals — Novel
1429 Homeostatic Machinery for Embryonic Development and Cancer Prevention.” *Current
1430 Opinion in Cell Biology* 48: 106–12.
1431 https://doi.org/https://doi.org/10.1016/j.ceb.2017.06.007.
1432 Marygold, Steven J., John Roote, Gunter Reuter, Andrew Lambertsson, Michael Ashburner,
1433 Gillian H. Millburn, Paul M. Harrison, et al. 2007. “The Ribosomal Protein Genes and
1434 Minute Loci of Drosophila Melanogaster.” *Genome Biology* 8 (10).
1435 https://doi.org/10.1186/gb-2007-8-10-r216.
1436 Matsuura, Shinya, Yoshiyuki Matsumoto, Ken Ichi Morishima, Hideki Izumi, Hiroshi Matsumoto,
1437 Emi Ito, Keisuke Tsutsui, et al. 2006. “Monoallelic BUB1B Mutations and Defective Mitotic-
1438 Spindle Checkpoint in Seven Families with Premature Chromatid Separation (PCS)

1439 Syndrome." *American Journal of Medical Genetics* 140 A (4): 358–67.
1440 https://doi.org/10.1002/ajmg.a.31069.
1441 McNamee, Laura M., and Michael H. Brodsky. 2009. "P53-Independent Apoptosis Limits DNA
1442 Damage-Induced Aneuploidy." *Genetics* 182 (2): 423–35.
1443 https://doi.org/10.1534/genetics.109.102327.
1444 Merino, Marisa M., Christa Rhiner, Jesus M. Lopez-Gay, David Buechel, Barbara Hauert, and
1445 Eduardo Moreno. 2015. "Elimination of Unfit Cells Maintains Tissue Health and Prolongs
1446 Lifespan." *Cell* 160 (3): 461–76. https://doi.org/10.1016/j.cell.2014.12.017.
1447 Morata, Ginés. 2021. "Cell Competition: A Historical Perspective." *Developmental Biology*.
1448 Elsevier Inc. https://doi.org/10.1016/j.ydbio.2021.02.012.
1449 Morata, Ginés, and Pedro Ripoll. 1975. "Minutes: Mutants of Drosophila Autonomously
1450 Affecting Cell Division Rate." *Developmental Biology* 42 (2): 211–21.
1451 https://doi.org/https://doi.org/10.1016/0012-1606(75)90330-9.
1452 Mukherjee, M., G. Ge, N. Zhang, D. G. Edwards, P. Sumazin, S. K. Sharan, P. H. Rao, D. Medina,
1453 and D. Pati. 2014. "MMTV-Espl1 Transgenic Mice Develop Aneuploid, Estrogen Receptor
1454 Alpha (ER)-Positive Mammary Adenocarcinomas." *Oncogene* 33 (48): 5511–22.
1455 https://doi.org/10.1038/onc.2013.493.
1456 Muller, Patricia A J, and Karen H. Vousden. 2014. "Mutant P53 in Cancer: New Functions and
1457 Therapeutic Opportunities." *Cancer Cell* 25 (3): 304–17.
1458 https://doi.org/10.1016/j.ccr.2014.01.021.
1459 Nagata, Rina, and Tatsushi Igaki. 2018. "Cell Competition: Emerging Mechanisms to Eliminate
1460 Neighbors." *Development Growth and Differentiation*. Blackwell Publishing.
1461 https://doi.org/10.1111/dgd.12575.
1462 Newsome, Timothy P., Bengt Åsling, and Barry J. Dickson. 2000. "Analysis of Drosophila
1463 Photoreceptor Axon Guidance in Eye-Specific Mosaics." *Development* 127: 851–60.
1464 Ni, Jian Quan, Rui Zhou, Benjamin Czech, Lu Ping Liu, Laura Holderbaum, Donghui Yang-Zhou,
1465 Hye Seok Shim, et al. 2011. "A Genome-Scale ShRNA Resource for Transgenic RNAi in
1466 Drosophila." *Nature Methods* 8 (5): 405–7. https://doi.org/10.1038/nmeth.1592.
1467 Nijhof, Joanne G W, Aat M Mulder, Ewoud N Speksnijder, Esther M Hoogervorst, Leon H F
1468 Mullenders, and Frank R de Gruijl. 2007. "Growth Stimulation of UV-Induced DNA Damage
1469 Retaining Epidermal Basal Cells Gives Rise to Clusters of P53 Overexpressing Cells." *DNA*
1470 *Repair* 6 (11): 1642–50. https://doi.org/https://doi.org/10.1016/j.dnarep.2007.05.008.
1471 Ochi, Naotaka, Mai Nakamura, Rina Nagata, Naoki Wakasa, Ryosuke Nakano, and Tatsushi Igaki.
1472 2021. "Cell Competition Is Driven by Xrp1-Mediated Phosphorylation of Eukaryotic
1473 Initiation Factor 2α." *PLoS Genetics* 17 (12).
1474 https://doi.org/10.1371/JOURNAL.PGEN.1009958.
1475 Ollmann, Michael, Lynn M Young, Charles J di Como, Felix Karim, Marcia Belvin, Stephanie
1476 Robertson, Kellie Whittaker, et al. 2000. "Drosophila P53 Is a Structural and Functional
1477 Homolog of the Tumor Suppressor P53." *Cell* 101: 91–101.
1478 Picco, V., and G. Pages. 2013. "Linking JNK Activity to the DNA Damage Response." *Genes &*
1479 *Cancer* 4 (9–10): 360–68. https://doi.org/10.1177/1947601913486347.
1480 Pilley, Steven, Tristan A Rodriguez, and Karen H Vousden. 2021. "Mutant P53 in Cell-Cell
1481 Interactions." *Gene & Dev* 35: 433–48. https://doi.org/10.1101/gad.347542.

1482 Riley, Todd, Eduardo Sontag, Patricia Chen, and Arnold Levine. 2008. "Transcriptional Control of
1483 Human P53-Regulated Genes." *Nature Reviews Molecular Cell Biology* 9 (5): 402–12.
1484 https://doi.org/10.1038/nrm2395.
1485 Rohr, Cristian O, R Gonzalo Parra, Patricio Yankilevich, and Carolina Perez-Castro. 2013.
1486 "INSECT: IN-Silico SEarch for Co-Occurring Transcription Factors." *Bioinformatics* 29 (22):
1487 2852–58. https://doi.org/10.1093/bioinformatics/btt506.
1488 Ruiz-Losada, Mireya, Raul González, Ana Peropadre, Alejandro Gil-Gálvez, Juan J. Tena, Antonio
1489 Baonza, and Carlos Estella. 2021. "Coordination between Cell Proliferation and Apoptosis
1490 after DNA Damage in Drosophila." *Cell Death and Differentiation*.
1491 https://doi.org/10.1038/s41418-021-00898-6.
1492 Sanchez, Juan A., Duarte Mesquita, Marýa C. Ingaramo, Federico Ariel, Marco Milan, and
1493 Andres Dekanty. 2019. "Eiger/TNFα-Mediated Dilp8 and ROS Production Coordinate Intra-
1494 Organ Growth in Drosophila." *PLoS Genetics* 15 (8).
1495 https://doi.org/10.1371/journal.pgen.1008133.
1496 Singla, Shruti, Lisa K. Iwamoto-Stohl, Meng Zhu, and Magdalena Zernicka-Goetz. 2020.
1497 "Autophagy-Mediated Apoptosis Eliminates Aneuploid Cells in a Mouse Model of
1498 Chromosome Mosaicism." *Nature Communications* 11 (1).
1499 https://doi.org/10.1038/s41467-020-16796-3.
1500 Snape, Katie, Sandra Hanks, Elise Ruark, Patricio Barros-Núñez, Anna Elliott, Anne Murray,
1501 Andrew H. Lane, et al. 2011. "Mutations in CEP57 Cause Mosaic Variegated Aneuploidy
1502 Syndrome." *Nature Genetics* 43 (6): 527–29. https://doi.org/10.1038/ng.822.
1503 Spradling, Allan C, Dianne Stern, Amy Beaton, E Jay Rhem, Todd Laverty, Nicole Mozden, Sima
1504 Misra, and Gerald M Rubin. 1999. "The Berkeley Drosophila Genome Project Gene
1505 Disruption Project: Single P-Element Insertions Mutating 25% of Vital Drosophila Genes."
1506 *Genetics* 153: 135–77. https://academic.oup.com/genetics/article/153/1/135/6047835.
1507 Struhl, Gary, and Konrad Basler. 1993. "Organizing Activity of Wingless Protein in Drosophila."
1508 *Cell*. Vol. 72.
1509 Sykiotis, Gerasimos P., and Dirk Bohmann. 2008. "Keap1/Nrf2 Signaling Regulates Oxidative
1510 Stress Tolerance and Lifespan in Drosophila." *Developmental Cell* 14 (1): 76–85.
1511 https://doi.org/10.1016/j.devcel.2007.12.002.
1512 Tanaka-Matakatsu, Miho, Jinhua Xu, Leping Cheng, and Wei Du. 2009. "Regulation of Apoptosis
1513 of Rbf Mutant Cells during Drosophila Development." *Developmental Biology* 326 (2): 347–
1514 56. https://doi.org/10.1016/j.ydbio.2008.11.035.
1515 Tian Xu, and Gerald M. Rubin. 1993. "Analysis of Genetic Mosaics in Developing and Adult
1516 Drosophila Tissues." *Development* 117: 1223–37.
1517 Titen, Simon W A, and Kent G. Golic. 2008. "Telomere Loss Provokes Multiple Pathways to
1518 Apoptosis and Produces Genomic Instability in Drosophila Melanogaster." *Genetics* 180
1519 (4): 1821–32. https://doi.org/10.1534/genetics.108.093625.
1520 Torres, Eduardo M, Tanya Sokolsky, Cheryl M Tucker, Leon Y Chan, Monica Boselli, Maitreya J
1521 Dunham, and Angelika Amon. 2007. "Effects of Aneuploidy on Cellular Physiology and Cell
1522 Division in Haploid Yeast." *Science* 317 (5840): 916–24. https://www.science.org.
1523 Tsurui-Nishimura, Noriko, Thanh Quang Nguyen, Tomonori Katsuyama, Tatsurou Minami,
1524 Hirofumi Furuhashi, Yoshiteru Oshima, and Shoichiro Kurata. 2013. "Ectopic Antenna
1525 Induction by Overexpression of CG17836/Xrp1 Encoding an AT-Hook DNA Binding Motif

1526 Protein in Drosophila." *Bioscience, Biotechnology, and Biochemistry* 77 (2): 339–44.
1527 https://doi.org/10.1271/bbb.120756.
1528 Uechi, Tamayo, Tatsuo Tanaka, and Naoya Kenmochi. 2001. "A Complete Map of the Human
1529 Ribosomal Protein Genes: Assignment of 80 Genes to the Cytogenetic Map and
1530 Implications for Human Disorders." *Genomics* 72 (3): 223–30.
1531 https://doi.org/10.1006/geno.2000.6470.
1532 Vishwakarma, Medhavi, and Eugenia Piddini. 2020. "Outcompeting Cancer." *Nature Reviews*
1533 *Cancer* 20 (3): 187–98. https://doi.org/10.1038/s41568-019-0231-8.
1534 Wagstaff, Laura, Maja Goschorska, Kasia Kozyrska, Guillaume Duclos, Iwo Kucinski, Anatole
1535 Chessel, Lea Hampton-O'Neil, et al. 2016. "Mechanical Cell Competition Kills Cells via
1536 Induction of Lethal P53 Levels." *Nature Communications* 7 (April).
1537 https://doi.org/10.1038/ncomms11373.
1538 Wei, Chia-Lin, Qiang Wu, Vinsensius B Vega, Kuo Ping Chiu, Patrick Ng, Tao Zhang, Atif Shahab,
1539 et al. 2006. "A Global Map of P53 Transcription-Factor Binding Sites in the Human
1540 Genome." *Cell* 124 (1): 207–19. https://doi.org/10.1016/j.cell.2005.10.043.
1541 Wells, Brent S., and Laura A. Johnston. 2012. "Maintenance of Imaginal Disc Plasticity and
1542 Regenerative Potential in Drosophila by P53." *Developmental Biology* 361 (2): 263–76.
1543 https://doi.org/10.1016/j.ydbio.2011.10.012.
1544 Wichmann, Anita, Burnley Jaklevic, and Tin Tin Su. 2006. "Ionizing Radiation Induces Caspase-
1545 Dependent but Chk2- and P53-Independent Cell Death in Drosophila Melanogaster."
1546 *Proceedings of the National Academy of Sciences* 103 (26): 9952–57.
1547 https://doi.org/10.1073/pnas.0510528103.
1548 Wichmann, Anita, Lyle Uyetake, and Tin Tin Su. 2010. "E2F1 and E2F2 Have Opposite Effects on
1549 Radiation-Induced P53-Independent Apoptosis in Drosophila." *Developmental Biology* 346
1550 (1): 80–89. https://doi.org/10.1016/j.ydbio.2010.07.023.
1551 Zhang, Bingqing, Sonam Mehrotra, Wei Lun Ng, and Brian R. Calvi. 2014. "Low Levels of P53
1552 Protein and Chromatin Silencing of P53 Target Genes Repress Apoptosis in Drosophila
1553 Endocycling Cells." *PLoS Genetics* 10 (9). https://doi.org/10.1371/journal.pgen.1004581.
1554 Zhang, Yinyin Xie, Ying Zhou, Cong Xiang, Lai Chen, Chenxi Zhang, Xiaoshuang Hou, Jiong Chen,
1555 Hui Zong, and Geng Liu. 2017. "P53 Pathway Is Involved in Cell Competition During Mouse
1556 Embryogenesis." *Proceedings of the National Academy of Sciences* 114 (3): 498–503.
1557 https://doi.org/10.1073/pnas.1617414114.
1558 Zhu, Lihua Julie, Ryan G Christensen, Majid Kazemian, Christopher J Hull, Metewo Selase
1559 Enuameh, Matthew D Basciotta, Jessie A Brasefield, et al. 2010. "FlyFactorSurvey: A
1560 Database of Drosophila Transcription Factor Binding Specificities Determined Using the
1561 Bacterial One-Hybrid System ." *Nucleic Acids Research* 39 (suppl_1): D111–17.
1562 https://doi.org/10.1093/nar/gkq858.
1563
1564
1565
1566
1567
1568